nature cell biology

Drosophila katanin is a microtubule depolymerase that regulates cortical-microtubule plus-end interactions and cell migration

Dong Zhang[1], Kyle D. Grode[2,5], Shannon F. Stewman[1,5], Juan Daniel Diaz-Valencia[3,5], Emily Liebling[1], Uttama Rath[1], Tania Riera[1], Joshua D. Currie[2], Daniel W. Buster[4], Ana B. Asenjo[1], Hernando J. Sosa[1], Jennifer L. Ross[3,5], Ao Ma[1,5], Stephen L. Rogers[2,5] and David J. Sharp[1,6]

Regulation of microtubule dynamics at the cell cortex is important for cell motility, morphogenesis and division. Here we show that the *Drosophila* katanin Dm-Kat60 functions to generate a dynamic cortical-microtubule interface in interphase cells. Dm-Kat60 concentrates at the cell cortex of S2 *Drosophila* cells during interphase, where it suppresses the polymerization of microtubule plus-ends, thereby preventing the formation of aberrantly dense cortical arrays. Dm-Kat60 also localizes at the leading edge of migratory D17 *Drosophila* cells and negatively regulates multiple parameters of their motility. Finally, *in vitro*, Dm-Kat60 severs and depolymerizes microtubules from their ends. On the basis of these data, we propose that Dm-Kat60 removes tubulin from microtubule lattice or microtubule ends that contact specific cortical sites to prevent stable and/or lateral attachments. The asymmetric distribution of such an activity could help generate regional variations in microtubule behaviours involved in cell migration.

Microtubules form complex and dynamic arrays with pivotal roles in the development and function of eukaryotic cells. Although microtubules are intrinsically dynamic, their cellular behaviours are tightly regulated by a host of other factors[1,2]. Thus, the microtubule cytoskeleton is responsive to a variety of cues and can locally adapt its dynamic properties accordingly. These regulatory inputs seem to be particularly relevant at the cell cortex, where localized alterations in microtubule dynamics and organization are central to cell migration, polarization, morphogenesis and division[3–6].

Katanin is a phylogenetically conserved enzyme that uses the energy of ATP hydrolysis to generate microtubule breakage *in vitro*[7]. Katanin was originally purified from sea urchin eggs as a heterodimer of p60, a catalytic subunit of relative molecular mass 60,000 (M_r 60, K) and p80, a targeting and regulatory subunit M_r (K) 80 (ref. 8). Katanin p60 and p80 homologues have now been identified in evolutionarily diverse systems and many organisms contain several genes encoding distinct p60 and/or p80 proteins. Functional analyses reveal diverse roles for katanin in mitosis and meiosis[9–12], in neuronal morphogenesis[13,14] and in the assembly and disassembly of cilia and flagella[15–18]. In addition, a katanin in higher plants has been shown to regulate the assembly of cortical microtubule arrays, which, in turn, determine the directional deposition of cellulose and thus impact cell morphogenesis[19–22]. In this context, katanin releases new microtubules nucleated from the walls of pre-existing microtubules[7,23].

We previously found that the *Drosophila* katanin p60, Dm-Kat60, associates with mitotic chromosomes and stimulates the depolymerization of kinetochore-associated microtubule plus-ends during anaphase A (ref. 12). In the present study, we tested the hypothesis that Dm-Kat60 also functions to regulate microtubule dynamics during interphase—a topic that has not been addressed in any other animal system.

RESULTS

Dm-Kat60 localizes at the interphase cell cortex

We first probed the localization of Dm-Kat60 in cultured interphase S2 cells using immunofluorescence. Dm-Kat60 immunostaining was found to be strongly enriched within a 0.5–3-μm-thick band extending around the entire cell boundary (Fig. 1a). This cortical staining pattern was reduced or abolished by Dm-Kat60 RNA interference (RNAi),

[1]Department of Physiology and Biophysics, Albert Einstein College of Medicine, 1300 Morris Park Avenue, Bronx, New York 10461, USA. [2]Department of Biology and the Center for Carolina Genome Sciences, University of North Carolina, Chapel Hill, 421 Fordham Hall, CB#3280, Chapel Hill, North Carolina 27599, USA. [3]Department of Physics, University or Massachusetts, Amherst, 302 Hasbrouck Laboratory, Amherst, Massachusetts 01003, USA. [4]Department of Cell Biology and Anatomy and the Arizona Cancer Center, University of Arizona, Tuscon, 1515 N. Campbell Avenue, Tuscon, Arizona 85724, USA. [5]These authors contributed equally to this work.
[6]Correspondence should be addressed to D.J.S. (e-mail: david.sharp@einstein.yu.edu)

Received 16 November 2010; accepted 7 January 2011; published online 6 March 2011; DOI: 10.1038/ncb2206

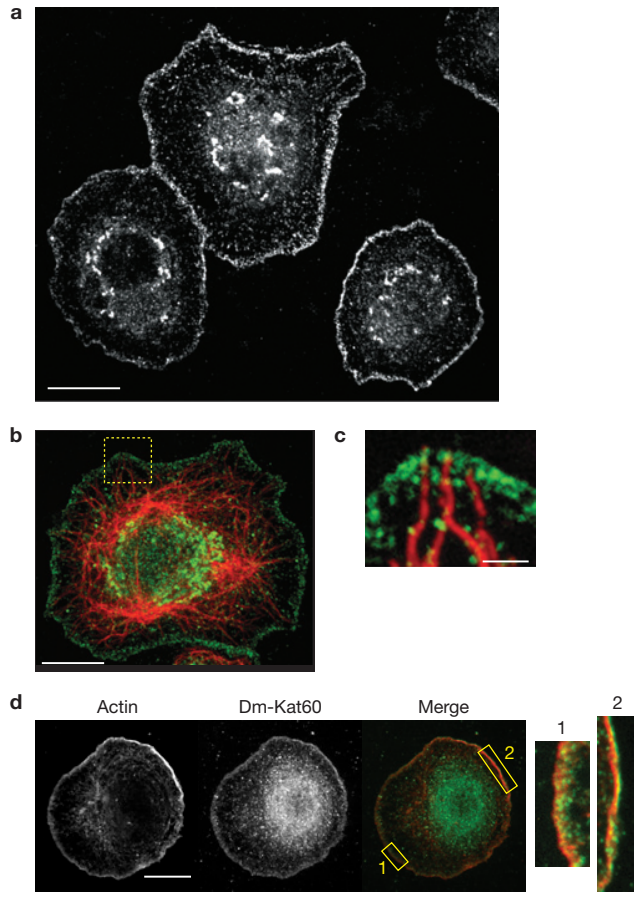

Figure 1 Dm-Kat60 targets the cell cortex of interphase cells. (**a**) Immunofluorescence micrograph showing the localization of Dm-Kat60 in interphase S2 cells (antibody characterized in ref. 12). (**b**) Immunofluorescence micrograph of an interphase S2 cell double labelled for microtubules (anti-α-tubulin; red) and Dm-Kat60 (green). (**c**) High magnification of the region outlined in **b**. (**d**) Immunofluorescence of an interphase S2 cell double labelled for actin (red) and Dm-Kat60 (green) and a higher magnification of the two regions outlined in the 'merge' panel. Scale bars, 10 μm (**a**,**b**,**d**), 2 μm (**c**).

supporting its specificity (see Supplementary Fig. S1a). Ectopically expressed Dm-Kat60 fused to green fluorescent protein (GFP) also acquired a cortical localization (see Supplementary Fig. S2a,b).

Although Dm-Kat60 showed little co-localization with microtubules in the interphase cell interior, numerous microtubule plus-ends were observed to extend into and terminate within the Dm-Kat60-rich cortical zone (Fig. 1b,c). Dm-Kat60 also generally co-localized with cortical actin (Fig. 1d). Cortical localization of Dm-Kat60 occurs independently of microtubules, as it persists following microtubule depolymerization with colchicine. However, it is nearly completely abolished when cells are treated with cytochalasin D, indicating a strong reliance on actin (see Supplementary Fig. S3). On the other hand, Dm-Kat60 RNAi did not prevent the cortical accumulation of actin (see Supplementary Fig. S1b).

Dm-Kat60 regulates interphase microtubules

We then carried out live analyses of microtubule dynamics in control and Dm-Kat60 RNAi-treated S2 cells expressing GFP–α-tubulin. In control cells, microtubules generally grew perpendicularly to the cortex, briefly paused on contacting the cortex and then underwent catastrophe (transition from growth to shrinkage) into the cell interior (Fig. 2a and Supplementary Movie S1a; see also ref.24). More than 90% of plus-end catastrophes (78 out of 84 observed in nine cells) occurred within 3 μm of the cell edge, indicating that the Dm-Kat60-rich cortical zone is a potential 'hotspot' for the induction of microtubule depolymerization.

Interestingly, some microtubules were also observed to break very near their ends on contacting the cortex. The newly formed plus-ends of these 'severed' microtubules initiated catastrophe immediately thereafter (Fig. 2b and Supplementary Movie S1c). Although such events were rarely observed when cells were imaged at 5 s intervals (our standard for longer time series), they appeared much more frequently when images were acquired at subsecond intervals (0.2–0.8 images per second). Under these conditions, putative severing events near microtubule tips preceded ~30% of observed catastrophes (20 out of 63 microtubule catastrophes observed in seven cells).

In stark contrast to controls, microtubules in most Dm-Kat60-depleted cells were noticeably curled beneath the cortex and often formed dense parallel arrays ringing the cell periphery (Fig. 2c and Supplementary Movie S1b). This phenotype was largely reversed by the induced expression of an RNAi-resistant Dm-Kat60-GFP construct (see Supplementary Fig. S2c,d). Although we were unable to observe the formation of these cortical arrays *de novo*, examination of the few clearly visible individual microtubules present at the onset of imaging provided insights into their genesis. Similarly to controls, these microtubules often contacted the cortex with their plus-end. However, instead of rapidly initiating catastrophe, they continued to grow along the cortex until they came into proximity with the underlying ring of microtubules, into which they were ultimately incorporated (Fig. 2d).

A unique role for Dm-Kat60 in microtubule dynamic instability

Approximately a quarter of the Dm-Kat60 RNAi-treated interphase S2 cells imaged contained at least some cortical domains with numerous unambiguously identifiable microtubule plus-ends. The dynamics of these were analysed in detail. To measure large numbers of plus-end dynamics, we developed an automated tracking algorithm that could accurately follow the position of microtubule ends over time (Fig. 3a and Supplementary Movie S1d,e; see Methods). The validity of this approach was confirmed by comparing a subset of microtubule trajectories generated automatically with those generated by hand (see Supplementary Fig. S4).

Consistent with our visual inspection of the data, control cells, most microtubule plus-end growth/shrinkage trajectories occurred along largely straight paths oriented perpendicular to the cortex (Fig. 3b). In contrast, Dm-Kat60 RNAi cells exhibited numerous plus-end trajectory paths parallel to the cortex (Fig. 3c). Moreover, on average, microtubule plus-ends in Dm-Kat60 RNAi cells spent significantly more time in growth (as opposed to shrinkage) parallel to the cortex and were positioned significantly closer to the cell edge (Fig. 3d,e).

We then analysed the life-history plots of the tracked microtubule plus-ends to specify the impact of Dm-Kat60 on dynamic instability (Table 1). As expected, Dm-Kat60 RNAi significantly suppressed plus-end catastrophes by more than twofold. Thus, Dm-Kat60 is normally a potent catastrophe promoter. Dm-Kat60 depletion also increased transitions from pause to growth; paused plus-ends were almost twice as likely to proceed to the growth state. Surprisingly, the frequency

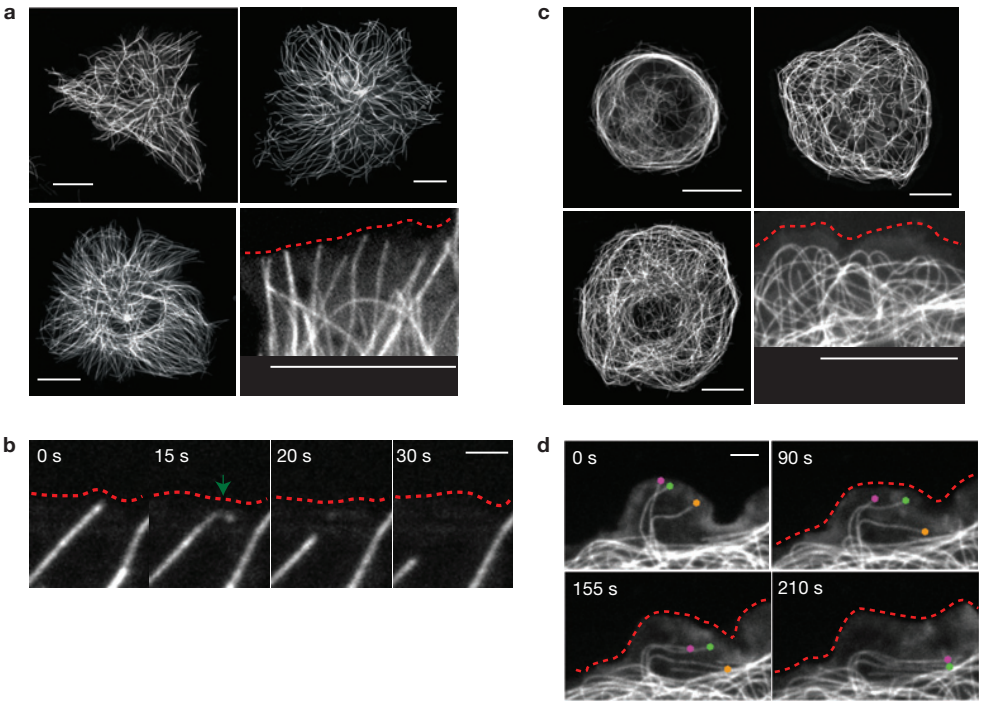

Figure 2 Depletion of Dm-Kat60 causes significant microtubule curling and bundling beneath the cortex. (**a**) Confocal images of live GFP–α-tubulin-expressing S2 cells treated with control RNA. The cell border is marked with a dashed red line in the higher-magnification image shown on the bottom right. The bottom right panel is also shown in Supplementary Movie S1a. (**b**) Time series of a putative microtubule-severing event at the cortex. The green arrow marks the site of microtubule breakage and the dashed red line marks the cell border. See also Supplementary Movie S1c. (**c**) Images of live GFP–α-tubulin-expressing S2 cells treated with Dm-Kat60 RNAi. As in **a**, the cell border is marked with a dashed red line in the higher-magnification image shown in the bottom right of this panel. This panel is also shown in Supplementary Movie S1b. (**d**) Time series of images obtained from a Dm-Kat60 RNAi-treated cell showing lateral growth of microtubule ends along the cortex and their subsequent incorporation into the underlying microtubule array. Individual ends are indicated by coloured circles and time (s) is labelled in each image. Scale bars, 10 μm (**a**,**c**), 1 μm (**b**), 2 μm (**d**).

of the reverse transition (a growing plus-end stalling into pause) also increased after Dm-Kat60 RNAi, but by a more modest 20%. Finally, we measured a slight (∼20%), but significant, increase in microtubule growth rate in Dm-Kat60 RNAi cells. On the other hand, depletion of Dm-Kat60 did not significantly impact the frequency of transitions out of the shrinkage state, nor did it alter the average rate of shrinkage.

The *Drosophila* kinesin-13 protein, kinesin-like protein 10A (KLP10A), has also been found to promote catastrophes at the cortex of interphase S2 cells[24]. To better understand the functional inter-relationship of Dm-Kat60 with this protein, we reassessed the influence of KLP10A on microtubule dynamics using our present methodologies (Table 1). As with Dm-Kat60 RNAi, the depletion of KLP10A significantly reduced the frequency of microtubule catastrophes. However, KLP10A RNAi also increased the frequency of transitions into pause, whereas Kat60 RNAi had the opposite effect. Also unlike Dm-Kat60 RNAi, KLP10A RNAi had no influence on microtubule growth rate, but strongly suppressed the rate of shrinkage.

Dm-Kat60 localizes at the leading edge of D17 cells and regulates their migration

The influence of Dm-Kat60 on microtubule dynamics at the cell cortex indicated a role in cell migration[25–28]. As S2 cells are immotile, we examined this possibility in migratory D17 cells. D17 cells were originally isolated from cultures of dissected imaginal discs[29]; despite their epithelial origin, D17 cells exhibit a gene-expression profile that is consistent with that of *Drosophila* haemocytes. Similarly to haemocytes[30–32], D17 cells spontaneously polarize in culture, assemble an exaggerated leading edge and exhibit robust cell motility (Supplementary Movie S2). Immunofluorescence revealed that Dm-Kat60 accumulates at the leading edge of polarized D17 cells, where it extensively co-localizes with actin (Fig. 4a). The other microtubule-severing enzymes in *Drosophila*, spastin and fidgetin[12,33], showed no such cortical enrichment, nor did their depletion obviously alter D17 cell migration (see Supplementary Fig. S5).

The influence of Dm-Kat60 on D17-cell migration was first examined in a wound-healing assay. D17-cell cultures were treated with Dm-Kat60 or control double-stranded RNA for 10 days, the confluent monolayers were wounded with a pipette tip and the resulting 'wounds' were imaged immediately or 24 h later. Unexpectedly, we measured a significant 1.4-fold increase in the rate of wound closure following Dm-Kat60 RNAi treatment (Fig. 4c,d). To specify the basis of this difference, we then assessed the intrinsic motility properties of single cells using time-lapse microscopy (Fig. 5a and Supplementary Movie S2). Dm-Kat60 RNAi-treated cells moved significantly faster than controls, with a striking increase in the number of high-velocity movements (Fig. 5b,c). They also exhibited an increase in total migration distance (Fig. 5d). Although control D17 cells do not exhibit directional motility in this assay, we did observe a slight, but significant, decrease in directionally persistent migration (Fig. 5e), indicating that the increased migration of Dm-Kat60 depleted cells in wound

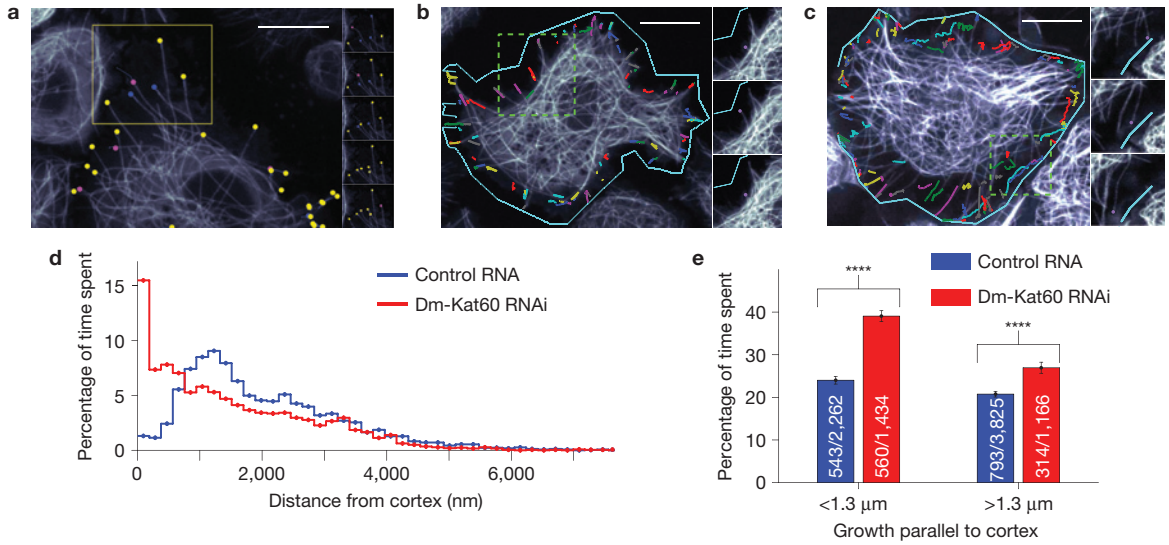

Figure 3 Automated tracking and quantitative analysis of microtubule plus-end organization and dynamics in control and Dm-Kat60 RNAi-treated cells. (**a**) Ends of GFP-labelled microtubules were tracked with an automated tracking algorithm. Each tracked microtubule end is marked with a coloured dot: growing ends in blue, pausing ends in yellow and shrinking ends in pink. The stack of panels on the right is a time series of the outlined region. (**b**) Trajectories of microtubule ends tracked in a control RNA-treated cell. Individual microtubule trajectory paths are indicated by coloured lines. (**c**) Trajectories of microtubule ends tracked in a Dm-Kat60 RNAi cell. Again, individual trajectory paths are indicated by coloured lines. Relative to controls, significantly more microtubules continue to grow after reaching the cortex, and so microtubules are frequently observed to bend and grow parallel to the cortex. (**d**) The microtubule ends in Dm-Kat60 RNAi cells (five cells, 494 microtubules, 6,087 distances) spent significantly ($P < 0.0001$) more time in the vicinity of the cortex, compared with control cells (seven cells, 257 microtubules, 2,600 distances). Microtubule ends within the cell interior could not be identified and thus were not analysed. (**e**) Cortical microtubules spend more time growing after Dm-Kat60 knockdown. The change in dynamic behaviour is most prominent in microtubule ends very near the cell margin (<1.3 μm), but is still significant ($P < 0.0001$) for ends further away (>1.3 μm). Numbers within bars indicate the number of frames in which microtubules grew parallel to the cortex/total number of frames observed. Error bars, s.e.m. Scale bars, 10 μm (all image panels).

healing assays does not result from increased directionality. Finally, we measured a notable difference in persistent migration following Dm-Kat60 RNAi treatment. Whereas migrating control cells spent ~63% of their time moving, cells depleted of Dm-Kat60 spent ~73% of their time migrating (Fig. 5f). Taken together, these data indicate that Dm-Kat60 normally serves as a negative regulator of cell motility by suppressing fast and persistent migration.

We also examined whether Katanin carried out a similar function in human cells. Although conventional human p60 had no apparent impact on cell movement, the p60-like protein KATNA1 (KL1; refs 34,35) localizes at the leading edge of migratory cells, regulates microtubule growth and negatively affects cell movement (see Supplementary Fig. S6a–e). Thus, human KATNA1 is potentially the functional orthologue of Dm-Kat60, at least during interphase.

Dm-Kat60 inhibits actin protrusions at the cell edge

Microtubules are believed to impact cell movement largely through the regulation of actin-based structures, such as lamellae[5,36–39]. Unfortunately, technical limitations precluded us from testing these cytoskeletal interactions in D17 cells. However, this could be studied in S2 cells co-expressing GFP–α-tubulin and mCherry–actin. Although Dm-Kat60 RNAi did not significantly impact on the accumulation of actin at the cortex or the rate of actin retrograde flow, it did strongly influence the cycles of lamellipodium protrusion and retraction. Specifically, Dm-Kat60 RNAi-treated cells showed a significant approximately threefold increase in the frequency of protrusions and a more than twofold increase in the average displacement per protrusion (Fig. 6b,c and Supplementary Movie S3). The increased cell-migration rates observed following Dm-Kat60 RNAi treatment could conceivably be due to a localized increase in the protrusion–retraction cycle at the leading edge.

Kat-60 is a microtubule-severing enzyme and a microtubule end depolymerase

Finally, we examined the *in vitro* mechanism of action of Dm-Kat60 using purified, baculovirus-expressed, recombinant GFP–Dm-Kat60 (rDm-Kat60). Taxol-stabilized, rhodamine-labelled microtubules were immobilized on coverslips[40], incubated with 50 nM rDm-Kat60 (Fig. 7a) and imaged over time using total-internal-reflection microscopy (TIRF). rDm-Kat60 robustly severed taxol-stabilized microtubules in the presence of ATP (Fig. 7b,c and Supplementary Movie S4), and this reaction was inhibited when ATP was depleted with hexokinase and glucose or replaced with the non-hydrolysable ATP analogue 5′-adenylyl-β-γ-imidiodiphosphate (AMPPNP; Fig. 7e). Thus, Dm-Kat60-mediated severing is stimulated by ATP hydrolysis. Severing also probably involves an interaction between Dm-Kat60 and the C-terminal tail of tubulin, because it was almost completely inhibited by the protease subtilisin, which removes the C termini of the tubulin subunits within the microtubule polymer. Subtilisin treatment was previously reported to inhibit katanin-mediated severing of microtubules[8].

To our surprise, we also observed substantial rDm-Kat60-induced depolymerization of microtubule ends, which generally preceded any obvious severing of the lattice (Fig. 7b,c). Similarly to severing, end depolymerization was suppressed by hexokinase and glucose, AMPPNP and subtilisin, indicating that both occur by a similar mechanism (Fig. 7e). Although both microtubule ends were depolymerized by

Table 1 Comparison of state-to-state frequency (no. s^{-1}) and growth/shrinkage rate (nm s^{-1}) between control, Dm-Kat60 RNAi and KLP10A RNAi cells.

State to state	Control RNA	Dm-Kat60 RNAi	KLP10A RNAi
G → S	0.0106 (34)*	0.0041 (7)	0.0028 (4)
	0.0072–0.0144†	0.0017–0.0081	0.0007–0.0073
		$P = 0.0249$ ‡	$P = 0.0004$***
G → P	0.0479 (167)	0.0576(75)*	0.0958 (116)
	0.0432–0.0522	0.0501–0.0645	0.0809–0.1053
		$P = 0.0225$*	$P = 0.0181$*
S → G	0.0098 (21)	0.0110 (10)	0.0045 (2)
	0.0063–0.0146	0.0056–0.0195	N/A
		$P = 0.7687$	N/A
S → P	0.0521 (109)	0.0590 (42)	0.1113 (47)
	0.0466–0.0575	0.0477–0.0678	0.0972–0.1242
		$P = 0.2084$	$P = 0.0035$**
P → G	0.0291 (72)	0.0481 (47)	0.0641 (60)
	0.0223–0.0369	0.0360–0.0627	0.0461–0.0817
		$P = 0.0145$*	$P = 0.1778$
P → S	0.0216 (77)	0.0156 (22)	0.0119 (14)
	0.0166–0.0275	0.0080–0.0263	0.0059–0.0237
		$P = 0.2657$	$P = 0.0031$**
Growth	52.79 (1,083)	62.13 (580)	58.68 (530)
	1.25§	1.97	1.73
		$P < 0.0001$****	$P = 0.033$*
Shrinkage	84.88 (819)	81.96 (316)	58.43 (179)
	2.81	4.61	3.63
		$P = 0.8380$	$P = 0.0001$***

*Numbers in parentheses indicate the event count in control RNA (five cells), Dm-Kat60 RNAi (seven cells) or KLP10A RNAi (five cells) treatment. †Intervals indicated are 95% confidence intervals calculated using a bootstrapping procedure with 1,000 resamples, and bias corrected and accelerated (BCa) correction. ‡Indicates statistically different from control if $P < 0.05$ (P values are shown). ** $P < 0.01$, *** $P < 0.001$, **** $P < 0.0001$. Statistical significance determined using a simulated two-tailed permutation test with 1,000 resamples. §s.e.m.

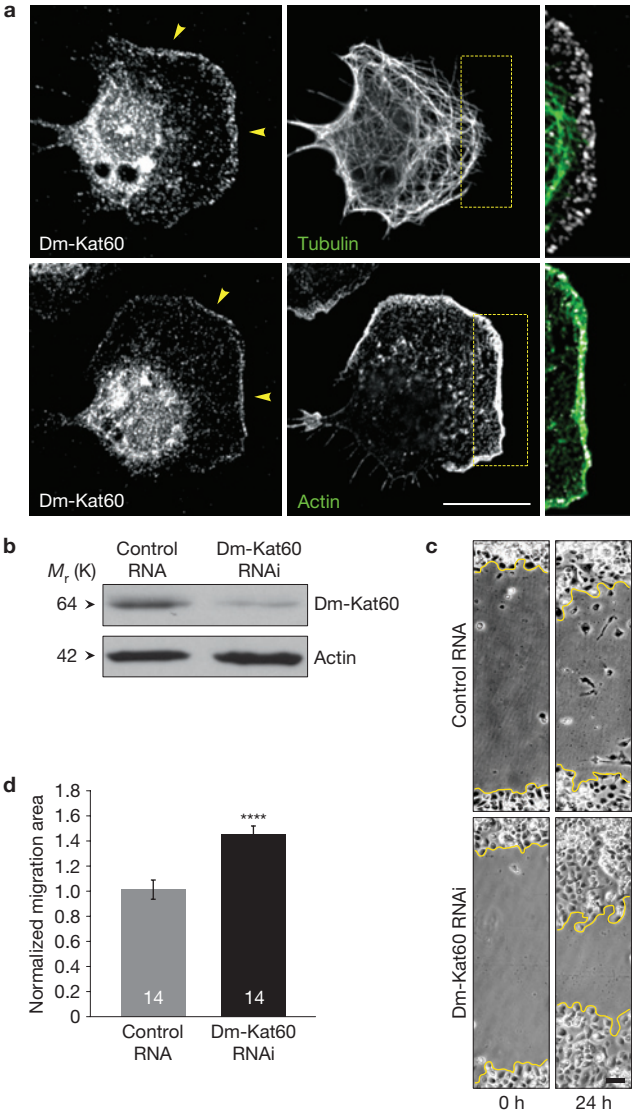

Figure 4 Dm-Kat60 targets to the leading edge of motile D17 cells and negatively regulates their migration. (**a**) Immunolocalization of Dm-Kat60, tubulin and actin in polarized *Drosophila* D17 cells. The arrowheads indicate enrichment of Dm-Kat60 at the leading edge; the outlined areas are magnified in the far right panels. (**b**) Western blot showing the depletion of Dm-Kat60 in D17 cells using RNAi. (**c**) Representative phase-contrast images of scratch-wounds at 0 and 24 h after wounding. (**d**) Quantification of migration during wound closure for control and Dm-Kat60 RNAi-treated D17 cells. Migration area was calculated by subtracting the total wound area at 24 h from the total wound area at 0 h after wounding and then normalized to control RNA. $P = 8.5 \times 10^{-5}$. Data represent mean values ± s.e.m. from four independent experiments. Numbers in bars are sample sizes. Scale bars, 10 μm (**a**), 50 μm (**c**). Uncropped images of blots are shown in Supplementary Fig. S8b.

rDm-Kat60, one end almost always depolymerized faster than the other (Fig. 7c). When these assays were carried out using polarity-marked microtubules, the plus-end was found to depolymerize approximately three times faster than the minus-end (Fig. 7d,e). To ensure that microtubule end depolymerization did not result from a protein contaminant, identical analyses were carried out using the catalytically inactive Dm-Kat60 (E393Q; ref. 41) mutant protein. The catalytically inactive Dm-Kat60 was entirely incapable of severing microtubules and, although it did induce some end depolymerization, the rate at which this occurred was approximately five times slower than that induced by the wild-type protein (Fig. 7e).

In a last set of experiments we examined the morphology of microtubule ends severed or depolymerized by rDm-Kat60 using electron microscopy. Samples of microtubules incubated with rDm-Kat60 and ATP, rDm-Kat60 and AMPPNP, and control microtubules without rDm-Kat60 were applied to electron microscopy grids and fixed by negative staining (Fig. 7f). We measured an approximate threefold increase in the number of microtubule ends per unit length in the rDm-Kat60/ATP condition relative to the AMPPNP and control samples without rDm-Kat60 (Fig. 7g) demonstrating that rDm-Kat60 was active in these assays. Interestingly, we observed no substantial difference in the morphology of microtubule ends among any of the above conditions. In all cases, microtubule ends were blunt or had a few straight protofilaments protruding from the end. In contrast, microtubules incubated with the *Drosophila* kinesin-13 KLP59D (ref. 42) showed numerous curled protofilaments peeling away from the ends (Fig. 7g), which is typical of kinesin-13-catalysed microtubule depolymerization[43]. This indicates that Dm-Kat60 and kinesin-13 proteins remove tubulin from microtubule ends by distinct mechanisms.

DISCUSSION

Our results identify Dm-Kat60 as an important regulator of microtubule dynamics and cell migration. The human katanin KATNA1 behaves similarly. In addition to its cellular roles, *in vitro* analyses indicate that Dm-Kat60 has the capacity to function

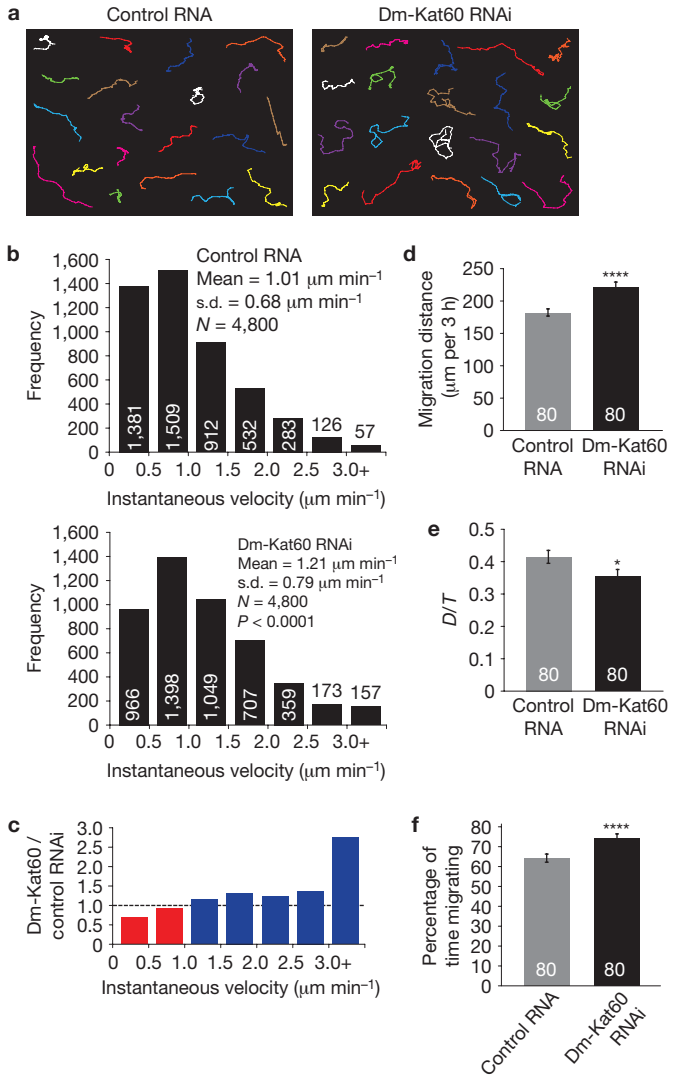

Figure 5 Dm-Kat60 negatively regulates multiple parameters of D17-cell motility. (**a**) Representative migration tracks of 20 cells for each treatment group (control and Dm-Kat60 RNAi; also see Supplementary Movie S2). (**b**) Frequency distributions of instantaneous cell velocities from time-lapse imaging of individual D17-cell movements. $P = 8.2 \times 10^{-40}$. (**c**) Quantification of the ratio of velocity frequencies between Dm-Kat60 and control RNAi treatments. The Dm-Kat60/control RNAi ratio was calculated by dividing the number of movements for Dm-Kat60 RNAi-treated cells by the number of movements for control RNA-treated cells for a given range of velocities from the graphs in **b**. A ratio less than one (red) represents a decreased number of movements for Dm-Kat60 RNAi relative to control RNA, and a ratio greater than one (blue) represents an increased number of movements for Dm-Kat60 RNAi relative to control RNA. Relative to control, Dm-Kat60 depletion decreases the frequency of cells migrating at low rates while increasing the frequency of high migration rates. (**d**) Quantification of total migration distance over a 3 h time period. $P = 1.5 \times 10^{-5}$. (**e**) Quantification of intrinsic cell directionality. Directionally persistent migration (D/T) was calculated as a ratio of the direct distance between start and end points (D) to the total migration distance (T). $P = 3.6 \times 10^{-2}$. (**f**) Quantification of persistent migration. The percentage of time that cells spent migrating was calculated by subtracting those movements between frames that were less than 2 μm (considered to be migratory pauses) from the total number of movements and then dividing by the total number of movements. $P = 3.7 \times 10^{-5}$. Data represent mean values ± s.e.m. from four separate double-stranded RNA treatments. Numbers in bars are sample sizes.

as both a microtubule-severing enzyme and a microtubule end depolymerase. On the basis of its cortical localization, RNAi phenotypes and catalytic activity, we propose that Dm-Kat60 (and KATNA1) contributes to the generation of a dynamic interface between the microtubule cytoskeleton and the interphase cortex by removing tubulin subunits from any region of the microtubule making contact with Dm-Kat60-rich cortical sites (see Supplementary Fig. S7).

Among the more unexpected outcomes of this study is the observation that Dm-Kat60 induces microtubule end depolymerization *in vitro*. However, given present models of the interaction of katanin with the microtubule, such a finding is not entirely surprising. Biophysical and biochemical studies have indicated that severing by katanin is mediated by the transient hexamerization of p60 proteins at the C terminus of a single tubulin within the microtubule[7,41]. ATP hydrolysis and/or the subsequent disassembly of the hexamer is believed to generate a mechanical force, which, through multiple iterations, induces the removal of the tubulin from the lattice. If katanin works by 'tugging' on a single tubulin heterodimer, then the exposed tubulins at the microtubule end are likely to be the easiest to remove because they lack a longitudinal contact. However, we cannot rule out the possibility that Dm-Kat60-mediated end depolymerization is a manifestation of multiple severing events occurring very near the tip.

Within the cell, the severing and depolymerase activities of Dm-Kat60 probably remain under very tight spatial constraints. In this regard, the recruitment of Dm-Kat60 to the cell cortex seems to be central to its interphase functions. Although our data indicate that this process is reliant on the presence of actin, but not microtubules, the specific mechanisms that deliver Dm-Kat60 to the cortex remain a mystery. One appealing hypothesis is that Dm-Kat60 is directly or indirectly linked to the cortical actin array through *Drosophila* p80. The p80 subunit contains repeated WD40 motifs known to mediate protein–protein interactions[44]. Similar motifs have been identified in some actin-binding proteins[45]. The WD40 repeats of p80 are essential for the centrosomal targeting of katanin in other organisms[46,47]. It has also been suggested that p60 acts independently of p80 in some circumstances[48]. The identification of the binding partners of Dm-Kat60 represents an important next step in understanding its cellular activities.

At the cortex, Dm-Kat60 suppresses microtubule growth primarily by inducing plus-end catastrophes and transitions from growth to pause. Although other classes of proteins are known to induce microtubule depolymerization, *in vitro*[43,49–51], the presumptive ability of Dm-Kat60 to remove tubulins from any region of the microtubule—end or lattice—may be particularly useful in the more complex cellular environment. For example, such an activity could enable Dm-Kat60 to prevent sustained microtubule growth along the cortex regardless of whether the microtubule contacts the cortex end-on or side-on. The newly created plus-end at the cortical-microtubule interface would then initiate catastrophe or enter the pause state depending on its association with other microtubule-binding proteins (see below). Moreover, the ends of polymerizing microtubules in cells are often 'capped' by plus-end-binding proteins such as EB1 (ref. 52). Dm-Kat60 could remove these by severing the microtubule at the base of the EB1 'cap' and/or directly removing EB1-bound tubulins from the plus-end. The acidic tail of EB1 could mimic the C terminus of tubulin, thereby providing a substrate for Dm-Kat60 (ref. 53).

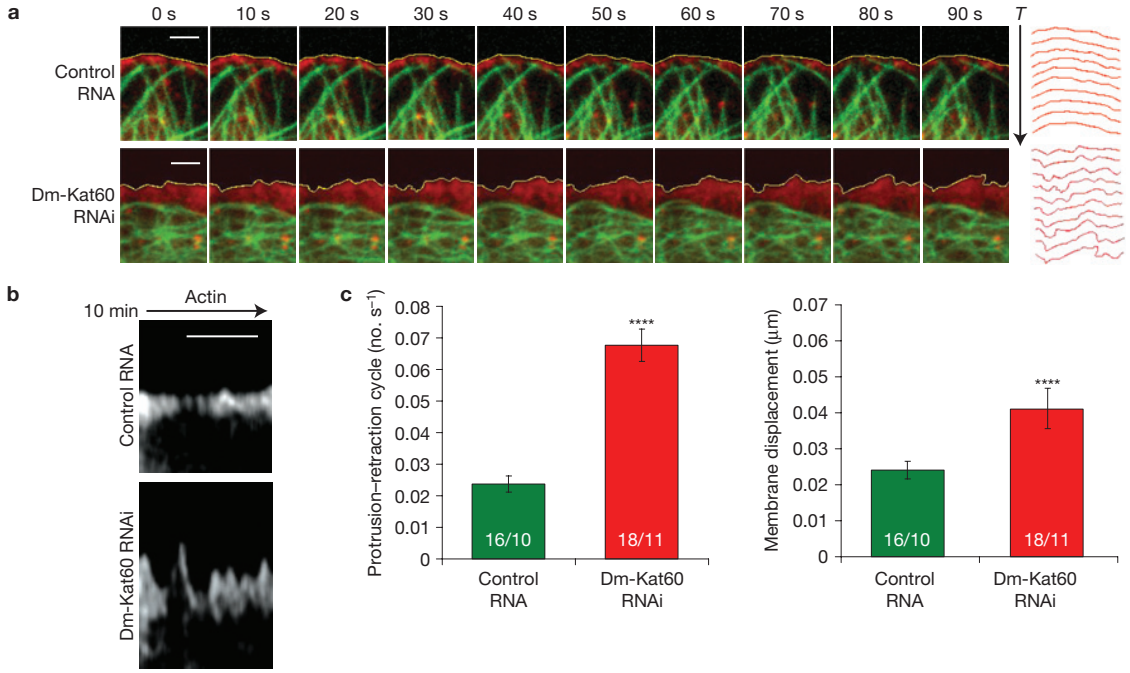

Figure 6 Dm-Kat60 negatively regulates actin protrusions at the cell edge. (**a**) Time-lapse images showing the cortical dynamics of control and Dm-Kat60 RNAi-treated S2 cells expressing GFP–α-tubulin and mCherry–actin. Yellow lines outline the edges of the cortical actin arrays in each image. These lines are stacked vertically (and shown in red) on the far right to illustrate the time-dependent alterations in the morphology of the cell edge (protrusions) in each condition (*T* labels the time axis). (**b**) Representative kymographs of mCherry–actin-labelled cortical regions from a control and Dm-Kat60 RNAi-treated cell. (**c**) Dm-Kat60 RNAi significantly increases both the frequency (left) and average displacement (right) of actin-based membrane protrusions ($P < 0.0001$ for both). Data represent mean ± s.e.m. and numbers in the columns indicate regions/cells analysed. Scale bars, 2 μm for **a** and **b**.

Of course, Dm-Kat60 is not alone in its ability to stimulate the catastrophe of microtubule plus-ends near the cortex of interphase S2 cells, as the *Drosophila* kinesin-13 KLP10A also shows this activity[24]. However, aside from the ability of both proteins to promote catastrophes, the activities of Dm-Kat60 and KLP10A are quite distinct. The most notable difference is that KLP10A does not concentrate on the cortex, but instead binds to the ends of polymerizing microtubules to which it is recruited by EB1. Intriguingly, recent work indicates that EB1 can inhibit the depolymerase activity of kinesin-13 proteins by shielding the plus-end[54]. If Dm-Kat60 were to generate plus-ends lacking EB1, then it could relieve this inhibition.

We propose that Dm-Kat60 and KLP10A work together as follows. (1) Dm-Kat60 removes tubulins (EB1 bound or otherwise) from regions of the microtubule that come in close proximity to the cortex, thereby creating a free plus-end at the cortical interface. Many of these newly created plus-ends immediately enter a paused state (depletion of EB1 has been shown to strongly promote pause[55]). (2) Next, KLP10A, which has already been accumulated near the end by EB1, promotes the transition of this end from pause to shrinkage—this transition can occur rapidly and may often appear as a catastrophe. Our present study also indicates that KLP10A increases the rate of plus-end depolymerization and thus a small, difficult-to-detect, portion of the protein may remain associated with the microtubule end as it depolymerizes. Why such an effect was not noted in our initial analysis of KLP10A is unknown, but may be due to the more limited region of the cortex analysed in that study[24].

The finding that Dm-Kat60 targets the leading edge of motile D17 cells and alters their migration provides a broader biological context through which our findings can be viewed and interpreted. Although the depletion of Dm-Kat60 had no obvious influence on the establishment of cell polarity, it did increase both the frequency and displacement of membrane protrusions, at least in S2 cells. The localized suppression of protrusions at the leading edge of motile D17 cells could exert negative control over the rate and persistence of cell movement.

The observation that Dm-Kat60 RNAi results in faster and more persistent migration seems consistent with other studies demonstrating that growing microtubules stimulate the GTPase Rac at the leading edge, which may promote adhesion-complex remodelling, needed to drive and sustain protrusions[38,39]. In addition, because Dm-Kat60 depletion at the leading edge of migratory cells should decrease catastrophes, microtubules could become unusually persistent and abundant in the extending protrusion, which may intensify other processes that favour protrusion, such as increased kinesin-mediated delivery of vesicles to the protrusion zone[56].

A recent study examining haemocyte migration in developing *Drosophila* embryos, for which we believe D17 cells to be a model, showed that haemocytes migrate less efficiently in response to guidance cues following the disruption of microtubule dynamics[30]. Under these conditions, the authors also observed an increase in cell velocities and a decrease in directional persistence, similar to D17 cells depleted of Dm-Kat60 by RNAi. Thus, Dm-Kat60 may modulate microtubule

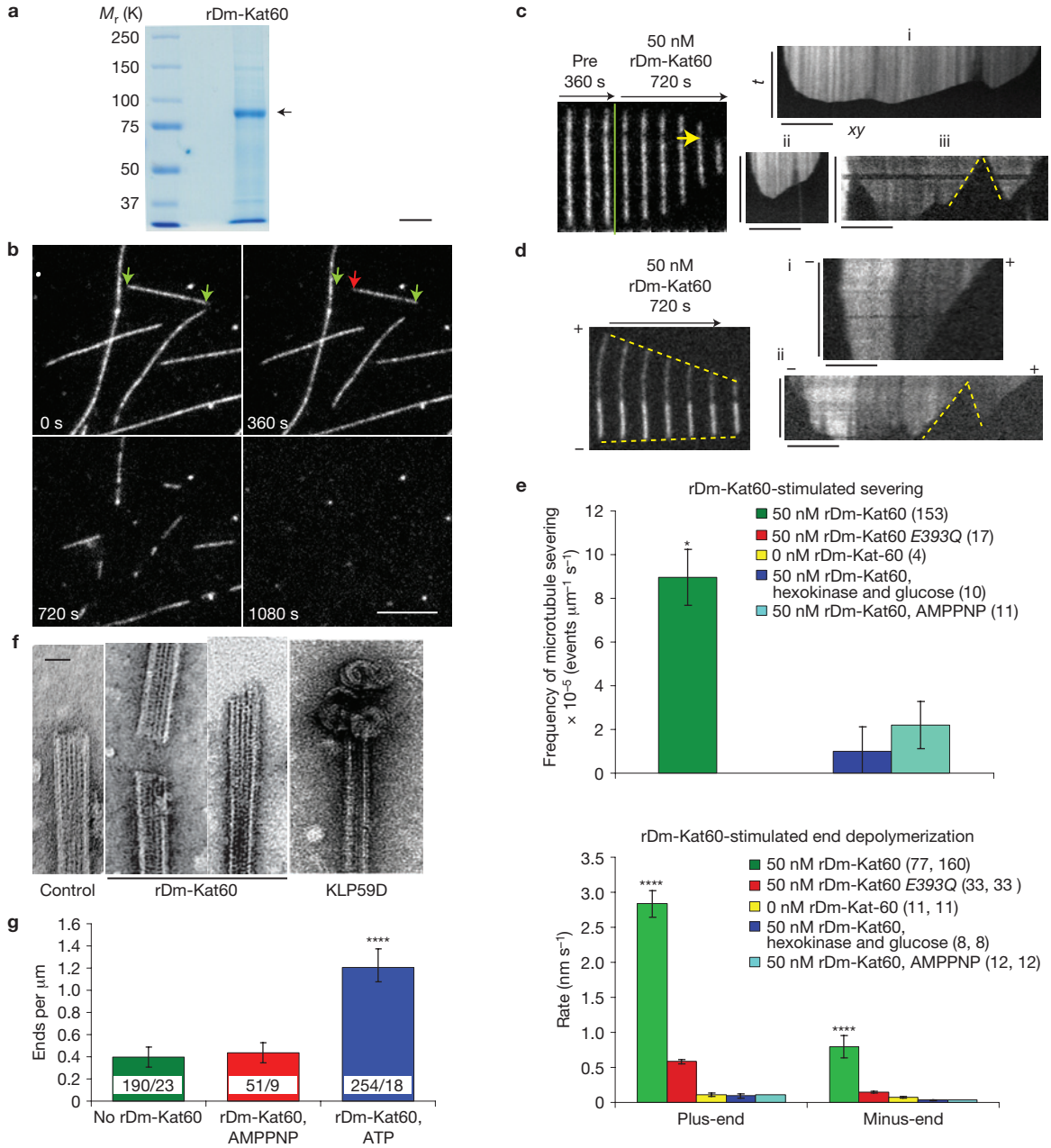

Figure 7 Dm-Kat60 severs and depolymerizes microtubules from their ends. (**a**) Coomassie-blue-stained SDS–polyacrylamide gel electrophoresis of the purified rDm-Kat60 protein used for analysis (see also Supplementary Fig. S8c). The arrow indicates the band corresponding to rDm-Kat60. (**b**) Time series of TIRF images showing the disassembly of a field of immobilized microtubules by 50 nM rDm-Kat60 and ATP. Green arrows mark the ends of an individual microtubule at the beginning of visualization; a red arrow marks a microtubule end that has shrunk from its initial position. Time (seconds) is indicated. (**c**) Left, time series of an individual microtubule (marked by arrows in **b**) before (pre) and after addition of rDm-Kat60. i–iii, Kymographs showing the depolymerization and severing (indicated by dotted yellow lines) of individual microtubules from other experiments. The time (t) axis is vertical and distance (x–y) axis horizontal in all kymographs shown in this figure. (**d**) Left, time series of an individual polarity-marked microtubule incubated with rDm-Kat60. The plus-end is dimly labelled and the minus-end is brightly labelled. i,ii, Kymographs showing the depolymerization and severing (dotted yellow lines) of further polarity-marked microtubules. (**e**) Upper, quantification of the frequency of microtubule severing by rDm-Kat60. All conditions included 2 mM ATP (or 2 mM AMPPNP). $P = 0.031$. Lower, measured rates of microtubule plus- and minus-end depolymerization by rDm-Kat60. $P = 3.1 \times 10^{-7}$. Again, all conditions included 2 mM ATP or AMPPNP. Data in both panels represent mean ± s.e.m. N = number of microtubules analysed. (**f**) Electron micrographs showing the ends of negatively stained microtubules after incubation with: no Dm-Kat60 (control), 50 nM rDm-Kat60 and 2 mM ATP (rDm-Kat60) or full-length KLP59D and ATP (KLP59D). (**g**) Quantification of microtubule ends per unit microtubule length. Compared with the no Dm-Kat60 and Dm-Kat60 (50 nM) + AMPPNP (2 mM) controls, Dm-Kat60 + ATP (50 nM GFP–Dm-Kat60, 2 mM ATP) induces three times more ends ($P < 0.0001$). Numbers in the column indicate numbers of microtubules/electron microscopy fields. Data represent mean ± s.e.m. pooled from two independent experiments. Scale bars, 500 μm (**a**), 10 μm (**b**), 20 nm (**f**).

dynamics at the leading edge to 'fine-tune' cell migration by suppressing protrusions.

The findings of this study uncover unexpected roles for the *Drosophila* katanin p60 Dm-Kat60 in the regulation of cortical microtubule dynamics and provide insights into how the microtubule cytoskeleton affects cell migration. The ability of cells to move and change shape is central to organismal development. Defects in these processes have been linked to human diseases such as cancer. Thus, our finding that human KATNA1 has many of the same functions as Dm-Kat60 suggests the former as a potentially useful therapeutic target. □

METHODS

Methods and any associated references are available in the online version of the paper at http://www.nature.com/naturecellbiology/

Note: Supplementary Information is available on the Nature Cell Biology website

ACKNOWLEDGEMENTS

D.J.S., U.R. and D.Z. were supported by NIH grant no. R01-GM065940 (to D.J.S.). S.L.R., K.D.G. and J.D.C. were supported by March of Dimes grant no. 1-FY08-429 and NIH grant no. R01 GM081645 (both to S.L.R.). S.F.S. and A.M. were supported by NIH grant no. R01-GM086536 (to A.M.). J.L.R. and J.D.D-V. were supported by March of Dimes grant no. 5-FY09-47 (to J.L.R.). H.J.S., A.B.A., E.L. and T.R. were supported by NIH grant no. R01-GM083338 (to H.J.S.).

AUTHOR CONTRIBUTIONS

D.Z. carried out and analysed most experiments using *Drosophila* S2 and human cells. D.Z. also purified and carried out the initial *in vitro* characterization of rDm-Kat60. K.D.G. carried out most experiments with *Drosophila* D17 under the direction of S.L.R.; J.D.C. also carried out analyses in D17 cells. S.F.S. designed the automated tracking algorithm under the direction of A.M. and used it to track microtubules in live-cell movies provided by D.Z.; J.D.D-V. and J.L.R. carried out numerous *in vitro* assays to quantify the microtubule-severing and end-depolymerase activities of rDM-Kat-60. A.B.A., E.L. and T.R. carried out and analysed the electron microscopy under the direction of H.J.S. U.R. carried out KLP59D for the electron microscopy assay. D.W.B. helped in the design of many experiments in S2 cells and made the model figure shown in Supplementary Information. D.J.S. wrote the manuscript (with the help of all authors, but particularly S.L.R.) and coordinated the efforts of the multiple laboratories involved in this project.

COMPETING FINANCIAL INTERESTS

The authors declare no competing financial interests.

Published online at http://www.nature.com/naturecellbiology
Reprints and permissions information is available online at http://npg.nature.com/reprintsandpermissions/

1. van der Vaart, B., Akhmanova, A. & Straube, A. Regulation of microtubule dynamic instability. *Biochem. Soc. Trans.* **37,** 1007–1013 (2009).
2. Jaworski, J., Hoogenraad, C. C. & Akhmanova, A. Microtubule plus-end tracking proteins in differentiated mammalian cells. *Int. J. Biochem. Cell Biol.* **40,** 619–637 (2008).
3. Martin, S. G. Microtubule-dependent cell morphogenesis in the fission yeast. *Trends Cell Biol.* **19,** 447–454 (2009).
4. Siegrist, S. E. & Doe, C. Q. Microtubule-induced cortical cell polarity. *Genes Dev.* **21,** 483–496 (2007).
5. Watanabe, T., Noritake, J. & Kaibuchi, K. Regulation of microtubules in cell migration. *Trends Cell Biol.* **15,** 76–83 (2005).
6. Siller, K. H. & Doe, C. Q. Spindle orientation during asymmetric cell division. *Nat. Cell Biol.* **11,** 365–374 (2009).
7. Roll-Mecak, A. & McNally, F. J. Microtubule-severing enzymes. *Curr. Opin. Cell Biol.* **22,** 96–103 (2010).
8. McNally, F. J. & Vale, R. D. Identification of katanin, an ATPase that severs and disassembles stable microtubules. *Cell* **75,** 419–429 (1993).
9. Buster, D., McNally, K. & McNally, F. J. Katanin inhibition prevents the redistribution of gamma-tubulin at mitosis. *J. Cell Sci.* **115,** 1083–1092 (2002).
10. McNally, K., Audhya, A., Oegema, K. & McNally, F. J. Katanin controls mitotic and meiotic spindle length. *J. Cell Biol.* **175,** 881–891 (2006).
11. Srayko, M., O'Toole, E. T., Hyman, A. A. & Muller-Reichert, T. Katanin disrupts the microtubule lattice and increases polymer number in *C. elegans* meiosis. *Curr. Biol.* **16,** 1944–1949 (2006).
12. Zhang, D., Rogers, G. C., Buster, D. W. & Sharp, D. J. Three microtubule severing enzymes contribute to the 'Pacman-flux' machinery that moves chromosomes. *J. Cell Biol.* **177,** 231–242 (2007).
13. Karabay, A., Yu, W., Solowska, J. M., Baird, D. H. & Baas, P. W. Axonal growth is sensitive to the levels of katanin, a protein that severs microtubules. *J. Neurosci.* **24,** 5778–5788 (2004).
14. Yu, W. *et al.* The microtubule-severing proteins spastin and katanin participate differently in the formation of axonal branches. *Mol. Biol. Cell* **19,** 1485–1498 (2008).
15. Casanova, M. *et al.* Microtubule-severing proteins are involved in flagellar length control and mitosis in Trypanosomatids. *Mol. Microbiol.* **71,** 1353–1370 (2009).
16. Quarmby, L. Cellular Samurai: katanin and the severing of microtubules. *J. Cell Sci.* **113Pt 16,** 2821–2827 (2000).
17. Rasi, M. Q., Parker, J. D., Feldman, J. L., Marshall, W. F. & Quarmby, L. M. Katanin knockdown supports a role for microtubule severing in release of basal bodies before mitosis in *Chlamydomonas*. *Mol. Biol. Cell* **20,** 379–388 (2009).
18. Sharma, N. *et al.* Katanin regulates dynamics of microtubules and biogenesis of motile cilia. *J. Cell Biol.* **178,** 1065–1079 (2007).
19. Stoppin-Mellet, V. *et al.* Arabidopsis katanin binds microtubules using a multimeric microtubule-binding domain. *Plant Physiol. Biochem.* **45,** 867–877 (2007).
20. Stoppin-Mellet, V., Gaillard, J. & Vantard, M. Katanin's severing activity favours bundling of cortical microtubules in plants. *Plant J.* **46,** 1009–1017 (2006).
21. Burk, D. H., Zhong, R. Q. & Ye, Z. H. The katanin microtubule severing protein in plants. *J. Integr. Plant Biol.* **49,** 1174–1182 (2007).
22. Burk, D. H., Liu, B., Zhong, R. Q., Morrison, W. H. & Ye, Z. H. A Katanin-like protein regulates normal cell wall biosynthesis and cell elongation. *Plant Cell* **13,** 807–827 (2001).
23. Nakamura, M., Ehrhardt, D. W. & Hashimoto, T. Microtubule and katanin-dependent dynamics of microtubule nucleation complexes in the acentrosomal *Arabidopsis* cortical array. *Nat. Cell Biol.* **12,** 1064–1070 (2010).
24. Mennella, V. *et al.* Functionally distinct kinesin-13 family members cooperate to regulate microtubule dynamics during interphase. *Nat. Cell Biol.* **7,** U235–U239 (2005).
25. Ozon, S., Guichet, A., Gavet, O., Roth, S. & Sobel, A. *Drosophila* stathmin: a microtubule-destabilizing factor involved in nervous system formation. *Mol. Biol. Cell* **13,** 698–710 (2002).
26. Lee, H. *et al.* The microtubule plus end tracking protein Orbit/MAST/CLASP acts downstream of the tyrosine kinase Abl in mediating axon guidance. *Neuron* **42,** 913–926 (2004).
27. Jankovics, F. & Brunner, D. Transiently reorganized microtubules are essential for zippering during dorsal closure in *Drosophila melanogaster*. *Dev. Cell* **11,** 375–385 (2006).
28. Borghese, L. *et al.* Systematic analysis of the transcriptional switch inducing migration of border cells. *Dev. Cell* **10,** 497–508 (2006).
29. Ui, K., Ueda, R. & Miyake, T. Cell lines from imaginal discs of *Drosophila melanogaster*. *In Vitro Cell Dev. Biol.* **23,** 707–711 (1987).
30. Stramer, B. *et al.* Clasp-mediated microtubule bundling regulates persistent motility and contact repulsion in *Drosophila* macrophages *in vivo*. *J. Cell Biol.* **189,** 681–689 (2010).
31. Kurtti, T. J. & Brooks, M. A. Growth and differentiation of lepidopteran myoblasts *in vitro*. *Exp. Cell Res.* **61,** 407–412 (1970).
32. Merchant, D., Ertl, R. L., Rennard, S. I., Stanley, D. W. & Miller, J. S. Eicosanoids mediate insect hemocyte migration. *J. Insect Physiol.* **54,** 215–221 (2008).
33. Roll-Mecak, A. & Vale, R. D. The *Drosophila* homologue of the hereditary spastic paraplegia protein, spastin, severs and disassembles microtubules. *Curr. Biol.* **15,** 650–655 (2005).
34. Torres, J. Z., Miller, J. J. & Jackson, P. K. High-throughput generation of tagged stable cell lines for proteomic analysis. *Proteomics* **9,** 2888–2891 (2009).
35. Sonbuchner, T. M., Rath, U. & Sharp, D. J. KL1 is a novel microtubule severing enzyme that regulates mitotic spindle architecture. *Cell Cycle* **9,** 2403–2411 (2010).
36. Waterman-Storer, C. *et al.* Microtubules remodel actomyosin networks in *Xenopus* egg extracts via two mechanisms of F-actin transport. *J. Cell Biol.* **150,** 361–376 (2000).
37. Watanabe, T., Noritake, J. & Kaibuchi, K. Roles of IQGAP1 in cell polarization and migration. *Novartis Found Symp.* **269,** 92–101 (2005).
38. Waterman-Storer, C. M. & Salmon, E. D. Actomyosin-based retrograde flow of microtubules in the lamella of migrating epithelial cells influences microtubule dynamic instability and turnover and is associated with microtubule breakage and treadmilling. *J. Cell Biol.* **139,** 417–434 (1997).
39. Waterman-Storer, C. M., Worthylake, R. A., Liu, B. P., Burridge, K. & Salmon, E. D. Microtubule growth activates Rac1 to promote lamellipodial protrusion in fibroblasts. *Nat. Cell Biol.* **1,** 45–50 (1999).
40. McNally, F. J. & Thomas, S. Katanin is responsible for the M-phase microtubule-severing activity in *Xenopus* eggs. *Mol. Biol. Cell* **9,** 1847–1861 (1998).
41. Hartman, J. J. & Vale, R. D. Microtubule disassembly by ATP-dependent oligomerization of the AAA enzyme katanin. *Science* **286,** 782–785 (1999).

42. Rath, U. *et al.* The *Drosophila* kinesin-13, KLP59D, impacts Pacman- and Flux-based chromosome movement. *Mol. Biol. Cell* **20,** 4696–4705 (2009).
43. Desai, A., Verma, S., Mitchison, T. J., Walczak, C. E. & Kin, I. Kinesins are microtubule-destabilizing enzymes. *Cell* **96,** 69–78 (1999).
44. Smith, T. F., Gaitatzes, C., Saxena, K. & Neer, E. J. The WD repeat: a common architecture for diverse functions. *Trends Biochem. Sci.* **24,** 181–185 (1999).
45. Hudson, A. M. & Cooley, L. Understanding the function of actin-binding proteins through genetic analysis of *Drosophila* oogenesis. *Annu. Rev. Genet.* **36,** 455–488 (2002).
46. Hartman, J. J. *et al.* Katanin, a microtubule-severing protein, is a novel AAA ATPase that targets to the centrosome using a WD40-containing subunit. *Cell* **93,** 277–287 (1998).
47. McNally, K. P., Bazirgan, O. A. & McNally, F. J. Two domains of p80 katanin regulate microtubule severing and spindle pole targeting by p60 katanin. *J. Cell Sci.* **113Pt 9,** 1623–1633 (2000).
48. Yu, W. *et al.* Regulation of microtubule severing by katanin subunits during neuronal development. *J. Neurosci.* **25,** 5573–5583 (2005).
49. Varga, V. *et al.* Yeast kinesin-8 depolymerizes microtubules in a length-dependent manner. *Nat. Cell Biol.* **8,** 957–962 (2006).
50. Gupta, M. L. Jr, Carvalho, P., Roof, D. M. & Pellman, D. Plus end-specific depolymerase activity of Kip3, a kinesin-8 protein, explains its role in positioning the yeast mitotic spindle. *Nat. Cell Biol.* **8,** 913–923 (2006).
51. Sproul, L. R., Anderson, D. J., Mackey, A. T., Saunders, W. S. & Gilbert, S. P. Cik1 targets the minus-end kinesin depolymerase kar3 to microtubule plus ends. *Curr. Biol.* **15,** 1420–1427 (2005).
52. Mimori-Kiyosue, Y., Shiina, N. & Tsukita, S. The dynamic behaviour of the APC-binding protein EB1 on the distal ends of microtubules. *Curr. Biol.* **10,** 865–868 (2000).
53. Mishima, M. *et al.* Structural basis for tubulin recognition by cytoplasmic linker protein 170 and its autoinhibition. *Proc. Natl Acad. Sci. USA* **104,** 10346–10351 (2007).
54. Montenegro Gouveia, S. *et al. In vitro* reconstitution of the functional interplay between MCAK and EB3 at microtubule plus ends. *Curr. Biol.* **20,** 1717–1722 (2010).
55. Rogers, S. L., Rogers, G. C., Sharp, D. J. & Vale, R. D. *Drosophila* EB1 is important for proper assembly, dynamics, and positioning of the mitotic spindle. *J. Cell Biol.* **158,** 873–884 (2002).
56. Reed, N. A. *et al.* Microtubule acetylation promotes kinesin-1 binding and transport. *Curr. Biol.* **16,** 2166–2172 (2006).

METHODS

S2 cell culture, RNAi and construction of plasmids. S2 cells expressing GFP–α-tubulin were a gift from R. Vale (University of California, San Francisco). Wild-type S2 cells were obtained from ATCC. Our methods for S2 cell culture, RNAi treatment of S2 cells and production of double-stranded RNA from the 3′ untranslated region of endogenous Dm-Kat60 (including sequences) have been described previously[12].

Immunofluorescence microscopy. S2 cells were plated on concanavalin-A-coated coverslips for 1.5 h, fixed in 100% methanol at −20 °C for 20 min and blocked with 5% normal goat serum in PBS containing 0.1% Triton X-100. Primary antibodies (Dm-Kat60, α-tubulin (DM1a, Sigma-Aldrich) and actin (clone C4, Millipore)) were applied at 1–20 μg ml^{-1} final concentration in blocking buffer. Fluorescent secondary antibodies (Jackson Immuno-Research Laboratories) were used at 7.5 μg ml^{-1}. Imaging was carried out on an Ultraview spinning-disc confocal system (PerkinElmer) mounted on an inverted microscope (Eclipse TE300; Nikon) with a 100× (1.4 NA) or 60× (1.4 NA) objective and captured with an Orca ER digital camera (Hamamatsu). For microtubule disruption, cells were treated with 50 μM colchicine for 18 h before fixation. For microfilament disruption, cells were treated with 5 μM cytochalasin D for 1 h before fixation.

Live-cell imaging and automated tracking. Four-dimensional time-lapse movies of GFP–α-tubulin-expressing S2 cells were acquired using the Ultraview spinning-disc confocal microscope described above. Microtubule ends were tracked through each series of time-lapse images with an automated tracking program using the following assumptions.

To define the tracking region, for each cell, we tracked microtubules in a hand-selected region of interest consisting of an outer (the cortex; Fig. 3a) and an inner (to avoid tracking into the crowded interior) boundary. For all calculations, the data from cells of the same treatment (control or Dm-Kat60 RNAi) were pooled.

To define growth and shrinkage, we calculated the angle α between the direction of the displacement of the microtubule tip and the direction of the microtubule itself. A value of $\cos(\alpha) > 0.2$ ($\alpha <\sim 78°$) indicated probable growth, and $\cos(\alpha) < -0.2$ ($\alpha >\sim 101°$) indicated probable shrinkage. These 'loose' cutoffs were chosen to deal with the curvature of microtubules in the Dm-Kat60 RNAi cells. To qualify as growing or shrinking, we required that the microtubule show the same behaviour (either growing or shrinking) for at least two consecutive frames, and that the overall displacement in a run of growth or shrinkage be at least 5 pixels.

The distance to the cortex was defined as the Euclidean distance from a microtubule tip to its closest point on the cortex. The difference in the distance distributions was tested using the Kolmogorov–Smirnov two-distribution test.

To define growth parallel to the cortex, for two consecutive frames t and $t+1$, the points on the cortex closest to the trajectory segment are given by $\mathbf{c}(t)$ and $\mathbf{c}(t+1)$, respectively, and the displacement vector along the cortex is $\delta\mathbf{c}(t) = \mathbf{c}(t+1) - \mathbf{c}(t)$. A microtubule was considered to grow parallel to the cortex if the angle between the tip displacement and $\delta\mathbf{c}(t)$ was less than 45°. Error bars plotted are the asymptotic standard errors for a binomial distribution: $\sqrt{p(1-p)/N}$, where p is the fraction that grow along the cortex, and N is the total number of data points. Significance was tested by χ^2 using a 2×2 table of dichotomous outcomes.

To calculate transition rates, catastrophes near the cortex were determined by counting the number of significant shrinkage events away from the cortex. To be counted, a shrinkage event had to begin within 0.63 μm of the cortex (10 pixels), and increase its distance from the cortex by at least 0.32 μm (5 pixels) by the end of the shrinkage run. The catastrophe statistic was calculated as

$$\frac{1}{N}\sum_{i=1}^{N}\left[\frac{[\text{depolymerization events in cell } i]/[\text{s in cell } i]}{[\text{microtubules near cortex in cell } i]}\right]$$

The standard error was estimated by bootstrap sampling on the terms of the sum with 1,000 resamples. Statistical significance was determined using 1,000 resamples of a one-sided permutation test with the test statistic $\log(S_{1,i}/S_{2,i})$, where $S_{1,i}$ and $S_{2,i}$ are the catastrophe statistic sums for resample i of control (1) and Dm-Kat60 RNAi (2), respectively. To calculate transition rates (Table 1), each frame of a microtubule trajectory was marked as either grow, shrink or pause. Grow and shrink states were defined as previously described. Pause was defined as neither growing nor shrinking. The lifetimes of states that began and ended in the middle of a trajectory (not on a boundary), as well as the state they transitioned to, were collected. The rate of transition between an initial state k (k = grow, shrink or pause) and a final state l ($l \neq k$) is

$$\frac{[\text{no. of transitions from } k \text{ to } l]}{[\text{no. of transitions out of } k]} \times \frac{1}{[\text{no. of transitions out of } k]}$$

$$\times \sum_i \left(\frac{1}{[\text{time in state } k \text{ before transition } i]}\right)$$

We used a bootstrap approximation to construct 95% confidence intervals of each transition, with 1,000 resamples of all lifetimes. Statistical significance was established using a two-sided permutation test with 1,000 resamples of the statistic $r_{1,i} - r_{2,i}$, where $r_{1,i}$ and $r_{2,i}$ correspond to the rates calculated in resample i of control (1) and Kat60-RNAi (2).

Purification of recombinant 6×His–GFP–Dm-Kat60. 6×His–GFP–Dm-Kat60 (rDm-Kat60) was cloned into pFastBac HTa (Invitrogen) and then transformed into DH10Bac *Escherichia coli* cells. The primers to amplify GFP were: forward, 5′-GAATTCACCATGGTGAGCAAGGGCGAGGAG-3′, and reverse, 5′-AAGGAAAAAAGCGGCCGCCTTGTACAGCTCGTCCATGCCGAG-3′. The primers to amplify Dm-Kat-60 were: forward, 5′-AAGGAAAAAAGCGGCCGCCA-CCATGTCCATAACCTTACTGCGAGGTGG-3′, and reverse, 5′-CCGCTCGAGTC-ATGACGATCCGAACTCCCTC-3′.

The bacmid was isolated from DH10Bac *E. coli* and then transfected into Sf9 cells. The virus-containing supernatant was used to infect fresh Sf9 cells for 72 h and the procedure was repeated twice to amplify the baculovirus. A 20 μl portion of the third-cycle supernatant was added to Sf9 cells in 250 ml SFM900-II medium (Invitrogen) with 5% fetal bovine serum to express 6×His–GFP–Dm-Kat60 at a low level (high levels of expression yielded inactive aggregates). Infected cells were lysed with a French press and centrifuged, and the resulting supernatant incubated with 1 ml nickel resin (Qiagen) at 4 °C for 1 h. The resin was then transferred into a 20 ml chromatography column (Biorad) and washed with four column volumes of wash buffer (40 mM imidazole in resuspension buffer without phenylmethylsulphonyl fluoride), and eluted with 500 mM imidazole in resuspension buffer without phenylmethylsulphonyl fluoride. The eluted rDm-Kat60 was concentrated by centrifugation and exchanged into severing buffer I (20 mM HEPES, at pH 7.0, 300 mM NaCl, 3 mM $MgCl_2$, 10% sucrose, 50 μM ATP, 5 mM dithiothreitol).

***In vitro* assays.** Rhodamine-labelled, taxol-stabilized non-polarity or polarity-marked nicrotubules were prepared according to an online protocol (http://mitchison.med.harvard.edu/protocols.html) and immobilized in the flow chamber with a kinesin rigor mutant (G234A) as reported[40]. The assay was conducted in severing buffer II (20 mM HEPES, at pH 7.0, 100 mM NaCl, 3 mM $MgCl_2$, 10% sucrose, 2 mM ATP, 10 mM dithiothreitol, 7.5 mg ml^{-1} bovine serum albumin, 0.1% Pluronic F-127) at 24 °C. An oxygen-scavenger system (220 μg ml^{-1} glucose oxidase, 22.5 mM glucose, 36 μg ml^{-1} catalase) was included to minimize photodamage. In some control assays, 5 mM AMPPNP or 4 mM hexokinase was used in place of ATP. Subtilisin pretreatment of microtubules was the same as reported in ref. 7. After perfusing microtubules into the flow-chamber cell, the purified rDm-Kat60 construct was introduced into the chamber and fluorescent microtubules were imaged by TIRF. Our TIRF microscope used a home-made laser system assembled around a Nikon Eclipse Ti microscope and a high-numerical-aperture objective (60×, NA = 1.49).

Digital images were saved as stacks of Tagged Image File Format files, and time-lapse series were saved as Audio Video Interleave files. Kymographs were generated using the Multiple Kymograph plug-in (ImageJ). From the kymographs of all microtubules recorded for each treatment of the depolymerization assay, we calculated the average angle of the microtubule ends' displacements through time. The depolymerization rate was determined by calculating the reciprocal of the tangent of the average angle, and then applying the appropriate conversions to derive the distance and time values. The *in vitro* severing frequency was determined by manually counting the number of severing events in every microtubule. The number of severing events in a single movie was divided by the total length of the microtubules at the start of the movie and divided by the total time of the movie.

D17-cell RNAi and migration assays. D17 cells were maintained in a room-temperature incubator in D17 medium: Schneider's medium (Invitrogen) supplemented with 10% fetal bovine serum (Gibco), 1% antibiotic–antimycotic (Gibco) and 1.25 μg ml^{-1} insulin (Invitrogen).

For RNAi, D17 cells were treated on days 0, 2, 4, 6 and 8 with 20 μg of dsRNA in 1 ml serum-containing Schneider cell medium (Life Technologies). On day 9, the RNAi-treated cells were plated on either extracellular-matrix-coated plastic tissue culture dishes for wound-healing experiments or extracellular-matrix-coated glass-bottom tissue culture dishes for single-cell analysis. For wound-healing experiments, cells were allowed to adhere for 4–6 h before manually scraping the cell monolayer with a pipette tip. After replenishing the medium, the scratch-wound regions were imaged 0 and 24 h after wounding using a phase-contrast microscope. For single-cell analysis, cells were imaged every 3 min for 3 h using a phase-contrast microscope equipped with a 10× (0.25 NA) objective.

Electron microscopy. Samples for negative-stain electron microscope experiments were prepared by mixing 1.5 μM of microtubules with 50 nM rDm-Kat60 in

DOI: 10.1038/ncb2206

severing buffer II (above) for 30 min at 24 °C. A 5 µl portion of this mixture was then loaded onto freshly glow-discharged carbon-supported grids (Electron Microscopy Sciences). The grid was washed and stained with 1% uranyl acetate, followed by observation in a Tecnai F20 microscope (FEI) operating at 120 kV with a nominal magnification of ×50,000.

Statistics. Differences between treatments were analysed using either a one-way nonparametric analysis of variance (Kruskal–Wallis) for multiple-group comparisons or a nonparametric *t*-test (Mann–Whitney) for two-group comparisons (SigmaStat, Systat Software; or GraphPad Prism, GraphPad Software). Measurement means were taken to be statistically different if $P < 0.05$.

nature cell biology

DOI: 10.1038/ncb2206

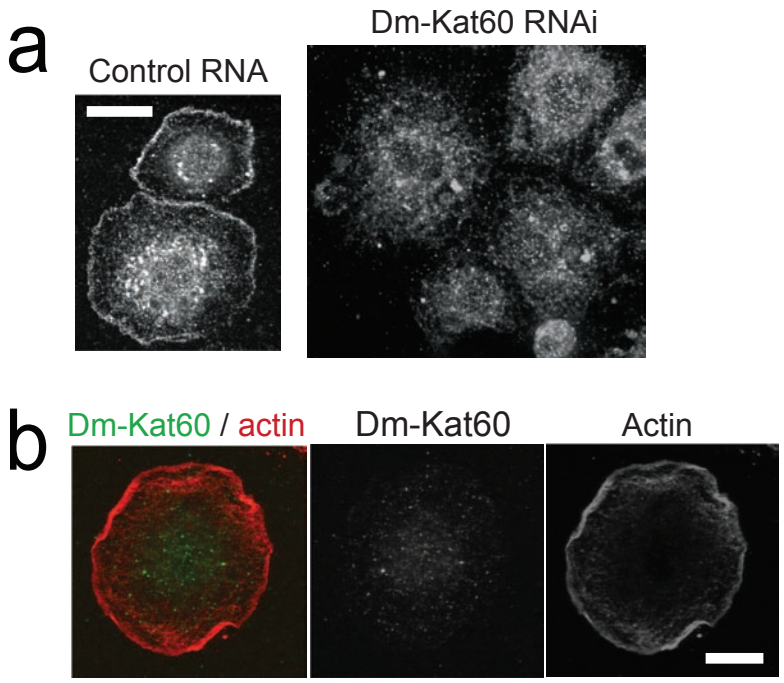

Figure S1 Dm-Kat60's cortical staining is reduced/abolished by Dm-Kat60 RNAi. (**a**) Comparison of Dm-Kat60 immunofluorescence in a field of control vs. Dm-Kat60 RNAi-treated S2 cells. Dm-Kat60's cortical staining pattern appears to be specific as it was significantly reduced or abolished by the targeted depletion of Dm-Kat60 by RNA-mediated interference. On average, Kat60 RNAi in S2 cells reduced the intensity of cortical Dm-Kat60 immunofluorescence by 71% relative to controls (100 randomly selected cells measured in each condition; $p<0.001$). Moreover, ~30% (31/100) of the RNAi-treated cells displayed no detectable Dm-Kat60 staining at the cortex compared to only 2% (2/100) of controls showing the same. (**b**) A Dm-Kat60 RNAi treated S2 cell double-labeled for Dm-Kat60 (green) and actin (red) further demonstrating that RNAi reduces the cortical staining of Dm-Kat60 but does not displace cortical actin. Scale bar, 10 μm (panels a and b).

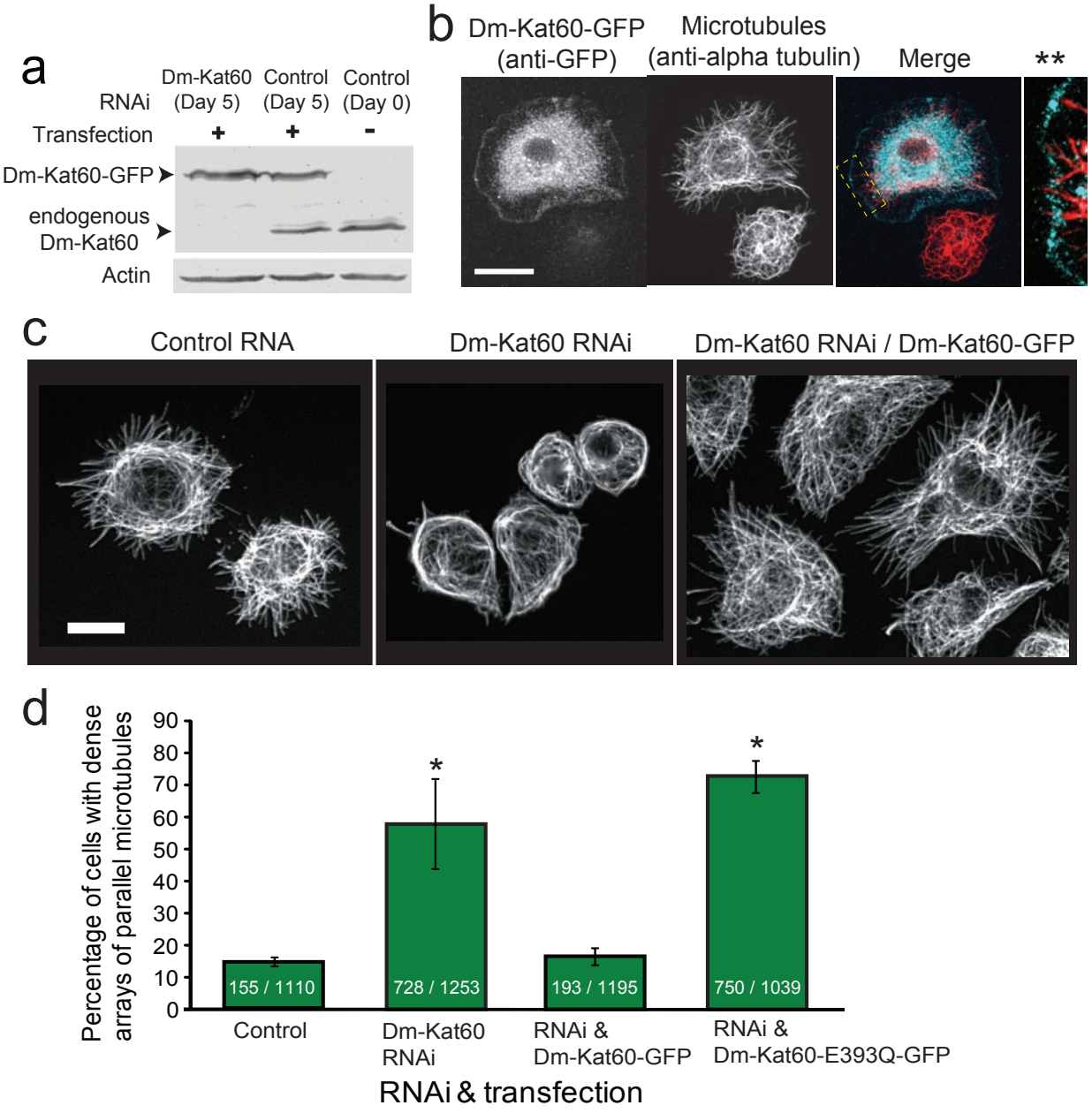

Figure S2 Ectopically expressed GFP-Dm-Kat60 localizes to the cortex of interphase S2 cells and rescues the Dm-Kat60 RNAi phenotype. (**a** & **b**) The cortical localization of Dm-Kat60 was confirmed in S2 cells expressing a Dm-Kat60-GFP fusion protein. Because overexpression of this construct is highly toxic to the cell, these experiments were performed in S2 cells depleted of endogenous Dm-Kat60 using dsRNA targeting the 3' untranslated region (UTR) of the Dm-Kat60 mRNA. RNAi-treated cells were then transfected with an inducible plasmid encoding Dm-Kat60 (lacking the endogenous 3'UTR) fused to GFP, which was expressed at a level approximating that of the endogenous protein. Panel a is a Western blot indicating endogenous Dm-Kat60 and Dm-Kat60-GFP expression levels following the indicated treatments. The lower anti-actin blot is included as a loading control (see also Supplemental information, Fig. S8a). Panel B shows shows the typical localization of Dm-Kat60-GFP (labeled with an anti-GFP antibody) and MTs (labeled with an anti-α-tubulin antibody) in a transfected interphase S2 cell. Far right panel (**) is a high magnification of the boxed region of the cell in the merged panel. Indirect immunofluorescence was used to localize GFP-Dm-Kat60 because the GFP signal alone was too low for the characterization of any specific localization pattern. Clearly apparent cortical staining was observed in ~67% (311/469) of Dm-Kat60-GFP transfected cells as compared to <5% (11/521) of non-transfected cells stained with the same antibody. (**c** & **d**) Replacement of endogenous Dm-Kat60 with the GFP-tagged fusion protein rescued the Dm-Kat60 RNAi phenotype. Panel C shows Immunofluorescence micrographs indicating the typical organization of MT arrays in control, Dm-Kat60 RNAi, and Dm-Kat60 RNAi / Dm-Kat60-GFP transfected interphase S2 cells. (**d**) Most Dm-Kat60 depleted cells have dense arrays of curled MTs arranged parallel to the cortex, but this phenotype is rescued once Dm-Kat60 RNAi cells are induced to express RNAi resistant Dm-Kat60-GFP. Rescue requires catalytically active Dm-Kat60, as demonstrated by the inability of the inactive mutant, Dm-Kat60 (E393Q)[41], to restore a normal cortical MT arrangement. $p = 0.0216$. Numbers in the columns indicate the number of cells containing a dense array of curled MTs/ total number of cells analyzed. Data represent Mean±SEM from three independent experiments. Scale bars, 10 μm (panels a and b).

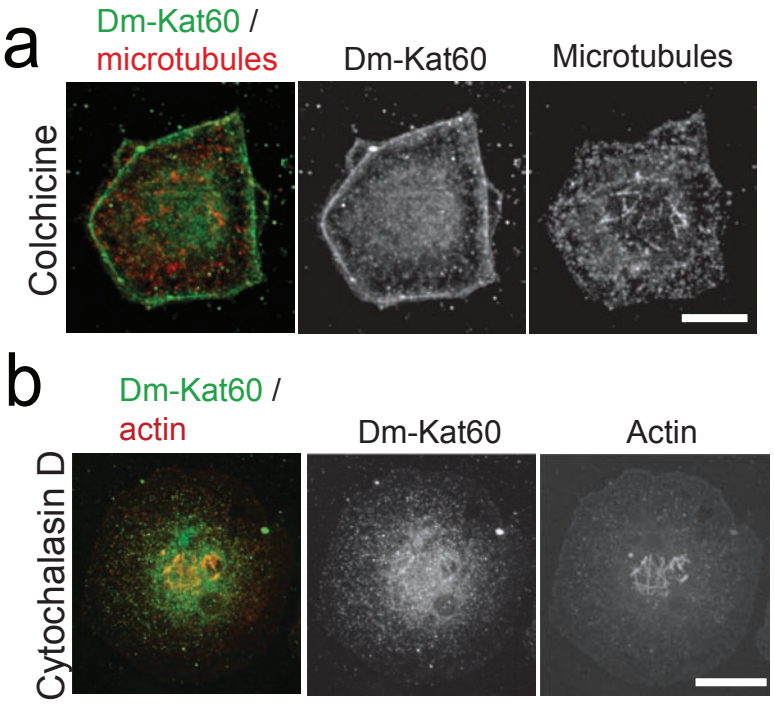

Figure S3 The cortical localization of Dm-Kat60 does not require MTs but is reliant upon actin. (**a**) Confocal micrographs showing that the localization of Dm-Kat60 at the cortex persists after microtubule disassembly with colchicine. (**b**) Cortical Dm-Kat-60 staining is lost when actin is disassembled by cytochalasin D. Scale bar, 10 μm (panels a,b).

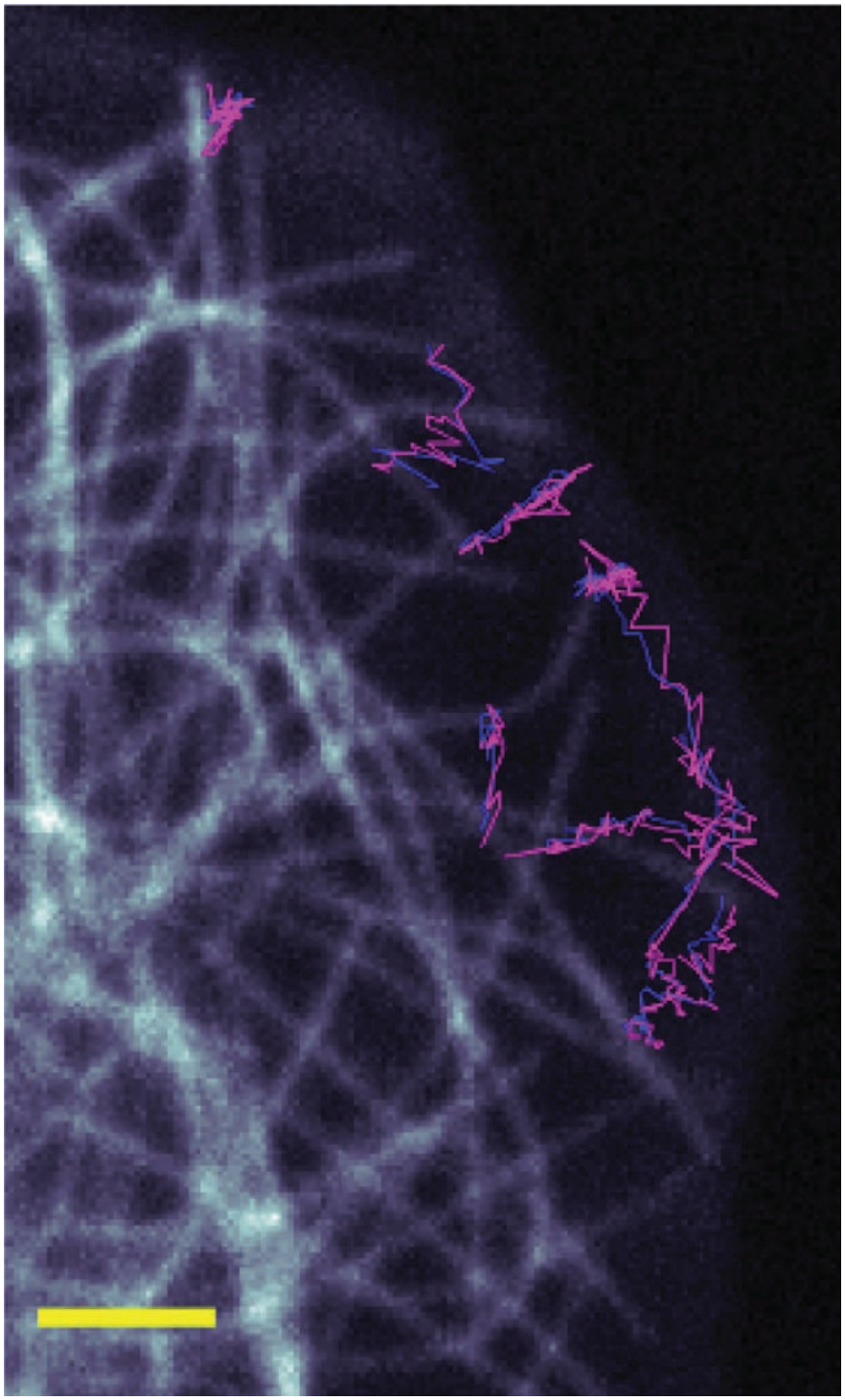

Figure S4 Comparison of MT plus-end trajectories generated using our automated algorithm vs. hand tracking. The image shows an individual time-point from a live cell movie of MT behaviors in a control GFP-α-tubulin-expressing interphase S2 cell. The trajectory paths of MT ends generated automatically are shown in magenta while the hand-tracked trajectory paths of these same MT ends are shown in blue. Scale bar, 5μm. In all, the automated algorithm correctly identified and followed the movement 98.3% of MT plus-ends (n=290).

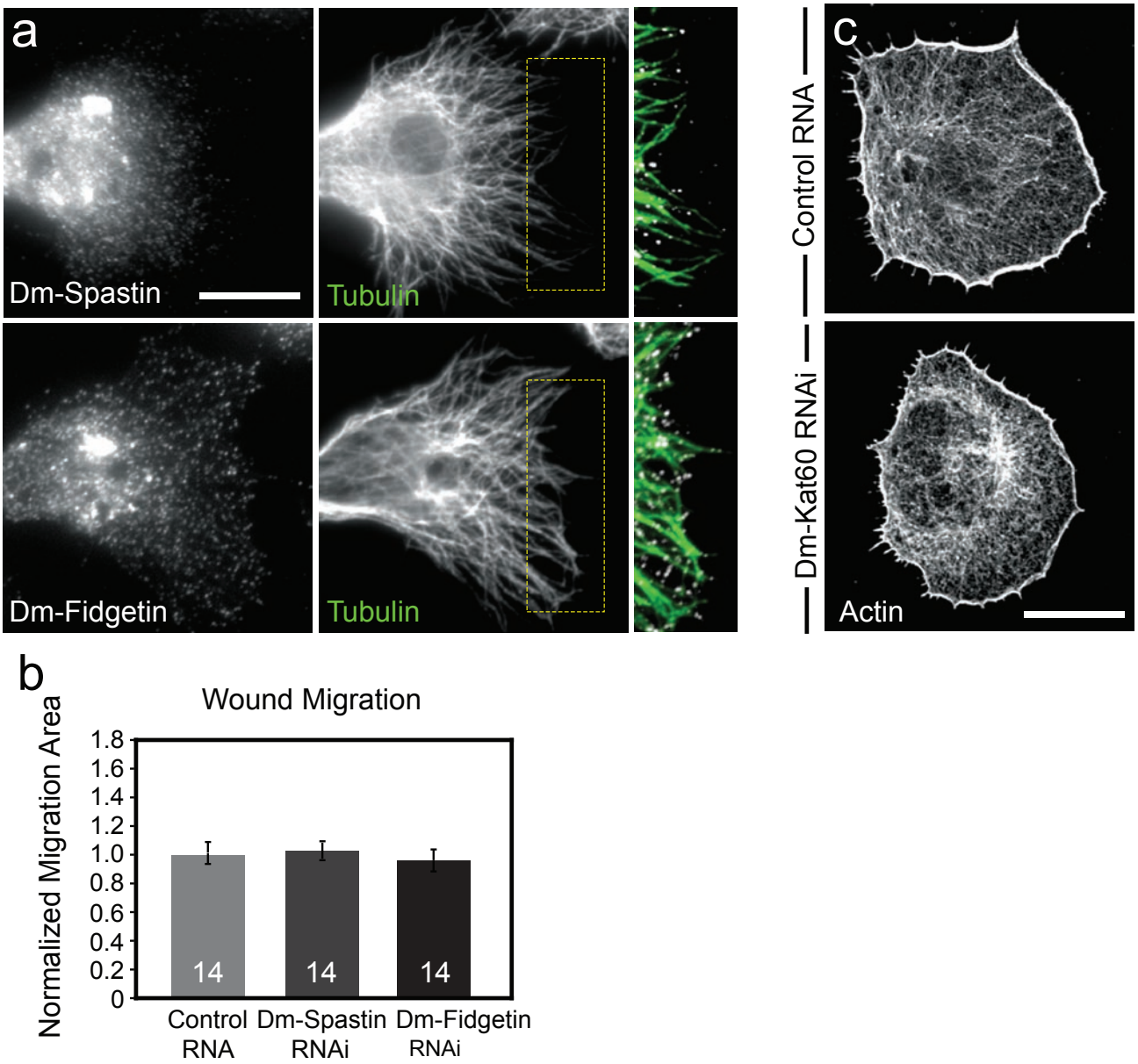

Figure S5 MT severing enzymes in D17 cells. (**a**) Immunolocalization of Spastin, Fidgetin, and tubulin in Drosophila D17 cells. The boxed areas are magnified in the insets. (**b**) Quantification of migration during wound closure for control, Spastin, and Fidgetin RNAi-treated D17 cells. Migration area was calculated by subtracting the total wound area at 24 hr from the total wound area at 0 hr after wounding and normalized to control RNAi. Data represent mean±SEM. (**c**) Immunolocalization of actin in control and Dm-Kat60 RNAi-treated D17 cells. Scale bars, 10 μm for both panel a and c

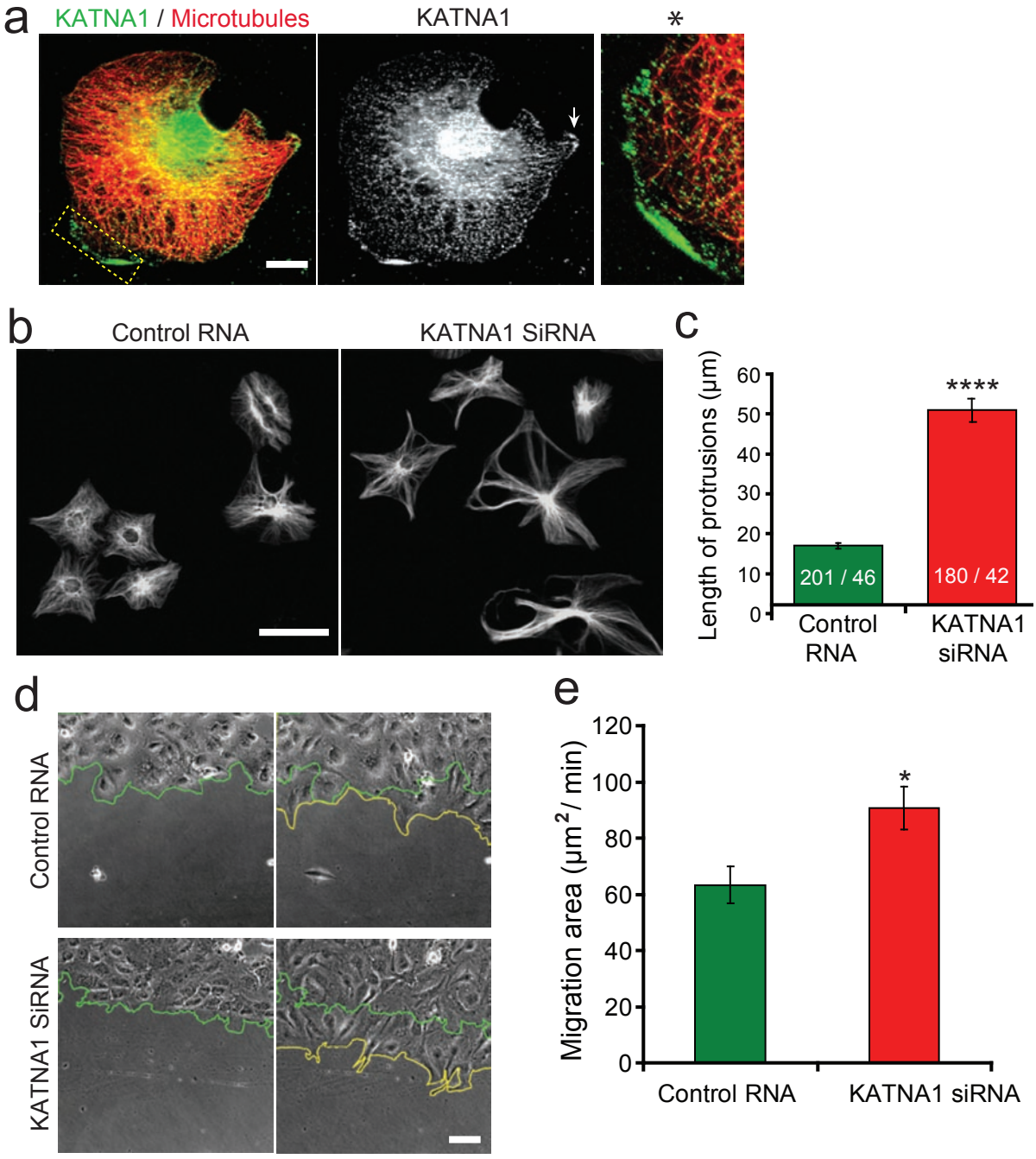

Figure S6 Human KATNA1 localizes to the leading edge of migratory cells and its depletion by RNAi affects microtubule organization and cell migration similarly to Dm-Kat60. (**a**) Immunofluorescence of human HS578T cells stained with our previously characterized anti-KATNA1 antibody[35] revealed that, similarly to Dm-Kat60, KATNA1 adopts a cortical localization that is most prominent at the leading edge of polarized cells as well as the edge of additional cellular protrusions (arrow). The area of the leading edge showing pronounced KATNA1 staining boxed in the merged panel is magnified in the inset. (**b**) SiRNA depletion of KATNA1 induces a dramatic alteration in cell morphology hallmarked by an increase in the length of cellular protrusions which filled with densely packed arrays of parallel MT. The image in this panel shows representative fields of control and KATNA1 siRNA-treated Hs578T cells immunostained for α-tubulin. (**c**) SiRNA depletion of KATNA1 increases the average length of the cellular protrusions more than 2-fold. $p < 0.0001$. Data represent mean±SEM. Numbers in the columns indicate the number of protrusions measured / total number of cells analyzed. (**d**) KATNA1 siRNA treated cells migrated ~1.5 fold faster than controls in wound healing assays. Monolayers of control and KATNA1 siRNA-treated Hs578T cells were wounded and imaged by phase microscopy immediately and 14 hrs later. The relative positions of the wound edge at the beginning and end of the experiment are indicated by green and yellow lines, respectively. (**e**) Quantification of the rate of wound closure in control vs. KATNA1 siRNA treated cultures. The data represent the mean±SEM of three independent experiments. $p = 0.0328$. Scale bar, 20 μm (panel a) or 100 μm (panels b, d).

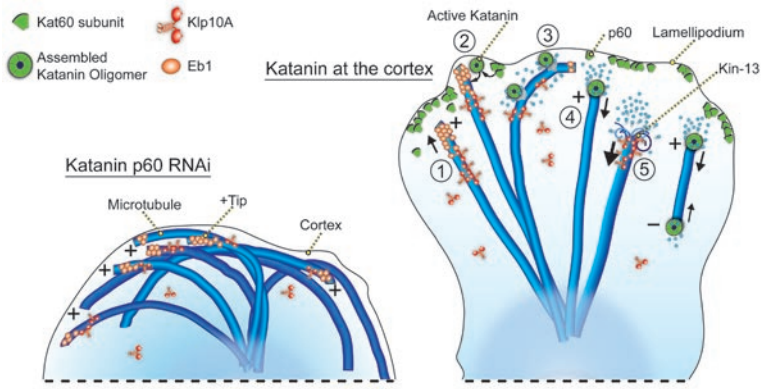

Figure S7 Model of kat-p60 activity at the cortex of interphase cells. Dm-Kat60 localizes to the cortex of lamellipodia (right), possibly by interacting with the F-actin enriched in this region. Our results suggest that as plus-ends of growing MTs approach the cortex, Dm-Kat60 attacks both the ends and the walls of MTs and perhaps eliminates stabilizing EB1 "caps" at plus-ends. Following Dm-Kat60 induced catastrophe and/or depolymerization at the cortex, kinesin-13 may assume responsibility for plus-end disassembly. If Dm-Kat60 is depleted (left), the loss of this potent catastrophe factor increases the lifetimes of MTs invading the cortex. Consequently, the MTs continue to grow even after reaching the cell boundary, and so the cell periphery fills with dense arrays of MTs running parallel to the cortex. MTs within these arrays could conceivably lose the ability to respond normally to the intra- and extra-cellular cues that optimize their dynamics and organization to stimulate movement, morphogenesis, etc…

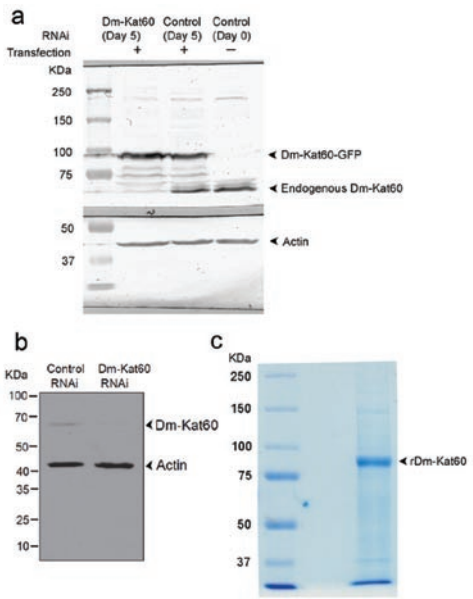

Figure S8. Electrophoretic data in uncropped form. Panel a shows the scanned image of the Western blot for Supplemental Figure S2a. To avoid cross reaction of different antibodies, the transferred membrane was cut into two parts and developed separately for Dm-kat60 / Dm-kat60-GFP or actin (arrows). Panel b shows the scanned image of the original of the original Western blot in Figure 4b. Dm-Kat60 and actin was detected at the same time (arrows). Panel c shows scanned image of the original SDS-PAGE of purified rDm-kat60 used in Figure 7a. Molecular markers are shown for each panel.

Supplemental Movie Legends

Movie S1 a &b: Time-series movie of MT plus-end dynamics near the cortex of a control (a) or Dm-Kat60 RNAi (b) treated GFP-tubulin expressing interphase S2 cell. Each image is a maximum intensity projection of three 1 µm optical sections; image stacks were collected at 5 second intervals. The cell was imaged using a 100X, 1.4 NA objective. **c:** Time-series movie showing severing near the plus-end of a MT at the cortex in a control treated GFP-α-tubulin expressing interphase S2 cell. Each image is a maximum intensity projection of three 1 µm optical sections and image stacks were acquired at three second intervals. **d & e**: Movie showing MT plus-ends tracked with our automated algorith in control (d) or Dm-Kat60 RNAi (e) treated S2 cells. Growing ends are marked with blue, shrinking ends with pink and pausing ends with yellow dots. The blue tail shows the last few frames of the trajectory. The time between frames is 5 seconds.

Movie S2 Time-series movies showing the motility of individual control (left) and Dm-Kat60 RNAi-treated (right) D17 cells imaged with a 10x phase contrast objective. 4 trajectories of individual cell movements are highlighted by colored lines in each field. Total time of imaging is 3 hours and time interval is 3 mins.

Movie S3 Time series movies showing representative cortical zones of S2 cells transfected with GFP-tubulin and mcherry-actin after control (left) or Dm-Kat60 RNAi (right) treatments. Cells were imaged with a 100X, 1.4 NA objective at 10 second intervals.

Movie S4 Time series of TIRF images showing rhodamine-labeled MTs fixed on a coverslip and incubated with 50 nM GFP-Dm-Kat60. Time in seconds is shown in the upper left of each image. Negative numbers indicate time before the introduction of Dm-Kat60 and positive numbers indicate time after the addition of Dm-Kat60. The movie is paused at t=0.